FORMATION OF PYRENE EXCIMERS IN MESOPOROUS ORGANICALLY MODIFIED SILICA THIN FILMS FOR VISUAL DETECTION OF NITROAROMATIC EXPLOSIVES

A THESIS SUBMITTED TO

MATERIALS SCIENCE AND NANOTECHNOLOGY PROGRAM

AND THE GRADUATE SCHOOL OF ENGINEERING AND SCIENCE

OF BILKENT UNIVERSITY

IN PARTIAL FULFILLMENT OF THE REQUIREMENTS

FOR THE DEGREE OF

MASTER OF SCIENCE

By

Pınar Beyazkılıç

August, 2013

I certify that I have read this thesis and that in my opinion it is fully adequate, in scope and in quality, as a thesis for the degree of Master of Science.

Assoc. Prof. Dr. Mehmet Bayındır (Advisor)

I certify that I have read this thesis and that in my opinion it is fully adequate, in scope and in quality, as a thesis for the degree of Master of Science.

Assist. Prof. Dr. Necmi Bıyıklı

I certify that I have read this thesis and that in my opinion it is fully adequate, in scope and in quality, as a thesis for the degree of Master of Science.

Assist. Prof. Dr. Hatice Duran

Approved for the Graduate School of Engineering and Science:

Prof. Dr. Levent Onural
Director of the Graduate School

ABSTRACT

FORMATION OF PYRENE EXCIMERS IN MESOPOROUS ORGANICALLY MODIFIED SILICA THIN FILMS FOR VISUAL DETECTION OF NITROAROMATIC EXPLOSIVES

Pınar Beyazkılıç
M.S. in Materials Science and Nanotechnology Program
Supervisor: Assoc. Prof. Dr. Mehmet Bayındır
August, 2013

Pyrene is a polycyclic aromatic hydrocarbon compound. Pyrene has been extensively applied as probing and sensing molecule because of excimer fluorescence which is formed upon interaction of two pyrene molecules in close proximity. In this thesis, we prepared porous thin films with bright pyrene excimer fluorescence and demonstrated their application in visual and rapid detection of nitroaromatic explosive vapors. The fluorescent films were obtained by physically encapsulating the pyrene molecules in the mesoporous organically modified silica (ormosil) networks which were synthesized via a facile template-free sol-gel method.

Formation and stability of pyrene excimers were investigated in both porous and nonporous ormosil thin films. Excimer emission was found to be significantly brighter and more stable in porous films compared to nonporous films. The excellent stability of the pyrene excimers in the porous films is due to the nanoscale confinement of pyrene molecules in the porous ormosil network. We studied the nitroaromatic explosive sensing performances of the pyrene doped porous films. Films exhibited a rapid and visible fluorescence quenching when they were exposed to TNT vapor. Fluorescence quenching efficiency of an approximately 100 nm thick porous film was calculated to be 55.6% after exposure to TNT vapor for 30 seconds revealing a rapid sensing behavior. Fluorescence quenching of the films can be easily observed under UV light enabling naked-eye detection of nitroaromatic explosives. A selective quenching was observed in the excimer emission against vapors of nitroaromatic molecules; trinitrotoluene (TNT), dinitrotoluene (DNT) and nitrobenzene (NB) among various aromatic and nonaromatic compounds. Furthermore, quenched excimer emission of the films can be recovered by simply washing the films with water. It is shown that the films can be reused

for at least five times after washing. To this respect, pyrene doped ormosil thin films can be presented as facile materials for nitroaromatic explosive sensing applications.

Keywords: Pyrene, excimer, ormosil, sol-gel, thin film, nitroaromatic explosive detection.

ÖZET

NİTROAROMATİK PATLAYICILARIN GÖZLE GÖRÜLEBİLİR TESPİTİ İÇİN MEZO BOŞLUKLU ORGANİK OLARAK MODİFİYE EDİLMİŞ SİLİKA İNCE FİLMLERDE PYREN EKZİMERLERİNİN OLUŞUMU

Pınar Beyazkılıç
Malzeme Bilimi ve Nanoteknoloji, Yüksek Lisans
Tez Yöneticisi: Doç. Dr. Mehmet Bayındır
Ağustos, 2013

Pyren çok halkalı aromatik bir hidrokarbon bileşiktir. İki pyren molekülünün çok yakın etkileşimiyle oluşan ekzimer ışımasından dolayı pyren, yaygın bir şekilde tespit edici ve algılayıcı molekül olarak kullanılmaktadır. Bu çalışmada, parlak pyren ekzimer ışımasına sahip mezo boşluklu ince filmler hazırlanmıştır ve bu filmlerin; hızlı ve gözle görülebilir nitroaromatik patlayıcı buharı tespitinde uygulaması gösterilmiştir. Işıyan filmler, pyren moleküllerinin basit bir sol-jel metoduyla kalıp molekül kullanmadan üretilen, mezo boşluklu organik olarak modifiye edilmiş silika (ormosil) yapıya fiziksel olarak hapsedilmesiyle elde edilmiştir.

Hem boşluklu hem de boşluksuz ormosil ince filmlerde pyren ekzimerlerinin oluşumu ve kararlılığı incelemiştir. Boşluklu filmlerde ekzimer ışımasının boşluksuz filmdekine oranla önemli derecede daha parlak ve daha kararlı olduğu görülmüştür. Pyren ekzimerlerinin boşluklu filmlerdeki beklenmedik kararlılığı, pyren moleküllerinin nano ölçekli boşluğa sahip ormosil yapıda sıkıştırılmasından kaynaklanmaktadır. Bu çalışmada, içine pyren hapsedilmiş boşluklu ve floresan filmlerin nitroaromatik patlayıcı algılama işlevleri incelenmiştir. Filmler, TNT buharına maruz bırakıldığında hızlı ve gözle görülebilir bir floresans sönümlenme göstermiştir. Yaklaşık 100 nm kalınlığındaki boşluklu bir filmin, 30 saniye boyunca TNT buharına maruz bırakıldıktan sonra floresans sönümlenme verimi % 55,6 olarak hesaplanmıştır. Filmlerin floresans sönümlenmesinin UV ışığı altında kolay bir şekilde gözlemlenebilmesi, nitrolu patlayıcıların çıplak gözle tespitine olanak sağlamaktadır. Ekzimer ışımasının, birçok aromatik ve aromatik olmayan bileşik arasında trinitrotoluen (TNT), dinitrotoluen (DNT) ve nitrobenzen (NB) gibi nitroaromatik bileşiklere karşı seçici özellik gösterdiği

gözlemlenmiştir. Ayrıca, filmlerin sönümlenmiş ekzimer floresansı; filmlerin su ile kolay bir şekilde yıkanmasıyla geri kazanılabilmektedir. Filmlerin en az beş kez yıkanıp tekrar kullanılabildiği gösterilmiştir. Bundan dolayı, pyrenli ormosil ince filmler nitroaromatik patlayıcı tespiti uygulamaları için basit malzemeler olarak sunulabilir.

Anahtar sözcükler: Pyren, ekzimer, ormosil, sol-jel, ince film, nitroaromatik patlayıcı tespiti.

Acknowledgement

I would like to thank my thesis supervisor Assoc. Prof. Mehmet Bayındır for his support, guidance and encouragement throughout my graduate studies. Also, I would like to thank Assist. Prof. Dr. Necmi Bıyıklı and Assist. Prof. Dr. Hatice Duran for attending my thesis committee.

I would like to thank my research group member Adem Yildirim for his helps during my studies. I would like to thank my other group members: Dilara Öksüz, Fahri Emre Öztürk, Bihter Dağlar, Erol Özgür, Mehmet Kanık, Hüseyin Duman, Tural Khudiyev, Ersin Hüseyinoğlu, Tamer Doğan, Gökçen B. Demirel, Emel Gürbüz, Neşe Özgür, Murat Dere, Muhammet Çelebi and M. Halit Dolaş for their helps. Additionally, I would like to thank former group member Hülya Budunoğlu for her supports.

I am grateful for my father Ahmet, my mother Aysel, my sister Betül and my brother Burak for their endless love and supports. Finally, I would like to thank Ahmet Dündar Sezer for his support and helps throughout my studies.

The financial support from TÜBİTAK and Turkish State Planning Agency is also gratefully acknowledged.

Dedicated to
my father and my mother

Contents

List of Figures

List of Tables

Chapter 1

Introduction

Pyrene and its derivatives, with their high quantum yield and chemical stability, are well-studied fluorophores for molecular labeling and fluorescent sensing applications [1, 2]. Pyrene has two main emission bands; first one is the emission of pyrene monomers (i.e., distance between molecules is larger than $\sim$1 nm) between 370 and 400 nm and second is the emission of pyrene excimers (i.e., distance is smaller than $\sim$1 nm) at around 470 nm [3]. The bright and visible emission of pyrene excimers is particularly interesting because it is very sensitive to the micro-environmental conditions such as temperature, pressure or pH [1]. In addition, the excimer emission can be affected by guest molecules and accordingly it can be used to detect various classes of chemicals including gases, organic molecules and metal ions [4, 5, 6, 7, 8, 9]. In particular, pyrene excimer emission can be rapidly quenched via exposure to nitroaromatic explosives based on electron-transfer between π-π^* stacked pyrene molecules and nitroaromatic molecules [10, 11, 12].

Therefore, thin films containing pyrene excimers are very promising materials as fluorescence sensors for numerous vapor phase analytes. However, preparation of thin films with strong pyrene excimer emission is challenging due to the easy dissociation of the pyrene excimers to monomers during solvent evaporation [13]. Most preferred method to prevent dissociation of excimers is covalent attachment of pyrene moieties to the thin film network [14]. Nevertheless, it is reported

that poor and unstable excimer formation can be observed even for the covalently bonded pyrene molecules [15]. Furthermore, covalent attachment of pyrene derivatives requires tedious and costly organic synthesis steps. Another method is the physical encapsulation of pyrene fluorophores during thin film preparation [11, 12, 14]. In order to observe excimer emission, polymers such as polystyrene (PS) or polyethersulfone (PES), which are structurally similar to pyrene must be used. In most of the studies, strong excimer emission is observed by using thin films prepared from these polymers. However, time-dependent excimer stability is not considered in these studies [11, 12, 16, 17]. Beside poor stability of excimer, another drawback of physical encapsulation method is the use of dense polymers as thin film networks. The analyte diffusion through the dense polymer matrix take very long times and as a result, sensing performances of the films decrease [18, 19, 20]. Very thin (< 100 nm) films can be prepared in order to eliminate this effect; however, measurements with very thin films are not reliable and reproducable due to low fluorescence signal [14]. Apparently, porous thin films where transport rate of analytes is higher and therefore fluorescence response is faster, are more suitable than their nonporous counterparts for vapor phase fluorescent sensing.

In this thesis, we report formation of pyrene excimers in porous thin films, to our knowledge, for the first time and their fluorescence quenching performance against nitroaromatic explosive vapors. We used mesoporous organically modified silica (ormosil) thin films, which were prepared using a facile template-free sol-gel method as porous scaffolds, and we physically encapsulated the pyrene molecules in the ormosil network during synthesis without making any chemical modification to the pyrene. We also investigated the stability of pyrene excimers in the porous ormosil films. It is important to note that although the dissociation of meta-stable pyrene excimers is very favorable in thin film systems, this phenomenon was rarely explored. In fact, the dissociation of pyrene excimers has been frequently used to evaluate the structure of the sol-gel materials [21, 22, 23, 24]. Surprisingly, we observed that the excimer emission is very stable in porous films (up to at least a week), whereas emission rapidly quenches in their nonporous counterparts within minutes. It is believed that the improved stability

of the pyrene excimers in porous films is due to the nanoscale confinement of the pyrene excimers in the porous ormosil network.

We analyzed the nitroaromatic explosive sensing performances of porous thin films for trinitrotoluene (TNT), dinitrotoluene (DNT) and nitrobenzene (NB). It is observed that fluorescence quenching efficiencies are as high as 18.2% and 19.9% for TNT and DNT, respectively, after ten seconds. The rapid fluorescence quenching of porous ormosil films can be observed visually under UV light. The selectivity of the sensor against nitroaromatic compounds was demonstrated by using vapors of various aromatic and nonaromatic molecules. Furthermore, quenched excimer emission of the porous ormosil films can be largely recovered by simply washing the films with water. Accordingly, we showed that the films are reusable at least for five quenching-recovery cycles.

Chapter 2

Basic Concepts and Review of the Literature

2.1 The Sol-Gel Process

Sol is composed of freely dispersed colloidal particles in a liquid whereas gel is a rigid network including interconnected particles and pores with submicrometer sizes. Sol-gel process represents the formation of a sol which then turns to a rigid gel network [25]. Sol-gel method is a versatile way with its mild operation conditions and high product yield. Since silica is one of the most widely used inorganic material, the sol-gel chemistry of silica is emphasized. Silica sol-gel process enables organic-inorganic hybrid materials synthesis which combines the stiffness of inorganic group (silica), chemical functionality and flexibility of organic groups. Organically modified silica materials can also be produced by encapsulating organic and organometallic species within sol-gel matrices by impregnation, physical entrapment and covalent bonding via the sol-gel process [26, 27].

Sol-gel process is composed of hydrolysis and condensation of liquid alkoxide precursors made of silicate monomers such as tetramethyl orthosilicate (TMOS) and tetraethyl orthosilicate (TEOS). The reactions of silicates are shown in Figure 2.1 [25]. Hydrolysis and condensation reactions of alkoxides are generally

Hydrolysis

$$\equiv Si\text{-}OR + H_2O \rightleftarrows \equiv Si\text{-}OH + R\text{-}OH$$

Esterification

Alcohol Condensation

$$\equiv Si\text{-}OR + HO\text{-}Si\equiv \rightleftarrows \equiv Si\text{-}O\text{-}Si\equiv + R\text{-}OH$$

Alcoholysis

Water Condensation

$$\equiv Si\text{-}OH + HO\text{-}Si\equiv \rightleftarrows \equiv Si\text{-}O\text{-}Si\equiv + H_2O$$

Hydrolysis

Figure 2.1: Reaction types of silicates.

carried out in the presence of catalyst such as acid or base in order to achieve high reaction rates. Silicate monomers are first hydrolyzed with water through an acid or base catalysed hydrolysis reaction as illustrated in Figure 2.2, where R is a functional (alkyl) group such as methyl or ethyl [28]. Alkoxide groups (OR) are replaced by hydroxyl groups (OH) during the hydrolysis step.

Then, hydrolyzed silicate monomers link their Si-OH group to Si-OH group of

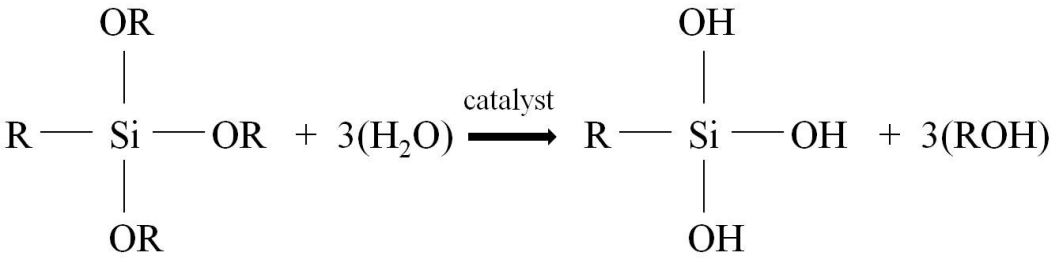

Figure 2.2: Hydrolysis mechanism for silicate monomers.

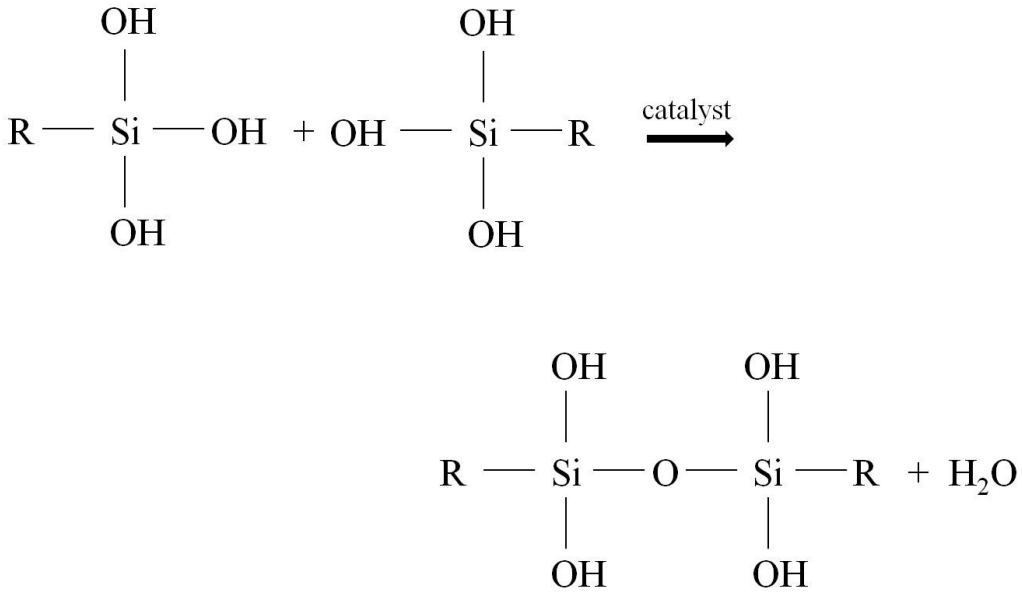

Figure 2.3: Condensation mechanism for silicate monomers.

another hydrolyzed monomer forming Si-O-Si (siloxane) bonds through the condensation reaction as illustrated in Figure 2.3. When the catalyst and monomers are mixed, hydrolysis and condensation reactions occur simultaneously at every site of the mixture. Linking of further Si-OH groups eventually forms SiO_2 network [28]. This resultant SiO_2 network exists as sol which includes submicrometer sized colloidal particles. The functional R groups which are individually linked to Si atoms in the initial monomer can not be hydrolized (Figure 2.3). As a result, they remain unchanged until the whole SiO_2 network forms which paves the way for the production of functional silica based materials by tuning the R groups.

2.2 Mesoporous Silica Materials

Mesoporous materials with their nanoporous characteristics and high surface area (1500 m^2/g) are used in various applications including catalysis, adsorption and sensor [26, 27]. These materials can have ordered or disordered pores with sizes varying between 2 and 50 nm [29]. Among all types of mesoporous materials,

silica based materials are one of the most widely used since they provide surface functionalization, optical transparency, robustness beside their porous nature. Mesoporous silica materials were firstly produced by Mobil Research and Development Corporation [30, 31]. Researchers described the family of M41S mesoporous materials with periodic pores. They also described MCM-41 structure from this family with hexagonally arranged structure and uniform pores whose sizes can be tailored from 1.5 nm to greater than 10 nm [30, 31].

Mesoporous silica based materials can be prepared via template based or template free approaches. Template-directed synthesis provides more ordered pore structure and tunable porosity in mesoporous silicas compared to template free method [26, 27]. Mesoporous silica materials have been applied in catalysis, adsorption, sensor, functional surface and biomedical applications [32, 33, 34, 35]. They can be produced in different forms in accordance with the desired application. In Figure 2.4 examples of the various mesoporous silica forms such as particle, thin film and aerogel are shown [34, 36, 37]. Mesoporous silica particles have been particularly applied in biomedical and sensor applications [34, 38]. Mesoporous silica thin films are produced by coating sol-gel derived sols on substrates by different techniques such as spin, spray and dip coating. Thin films are generally used for functional surface preparation [35]. Finally, aerogels are produced by drying the sol-gel derived wet silica gels at supercritical conditions. Aerogels are considered as insulation materials and hosts for many organic and inorganic molecules [39, 40].

2.2.1 Template Based Preparation of Mesoporous Silica Materials

Template based mesoporous silicas with ordered structure and uniform pore size varying in the range of 2-30 nm are produced from alkoxide monomers (TMOS or TEOS) via surfactant templating approach. In Figure 2.5, the mechanism for the formation of mesoporous silica network by surfactant-directed approach is shown [41, 42]. Basically, surfactant molecules interacts with alkoxide monomers

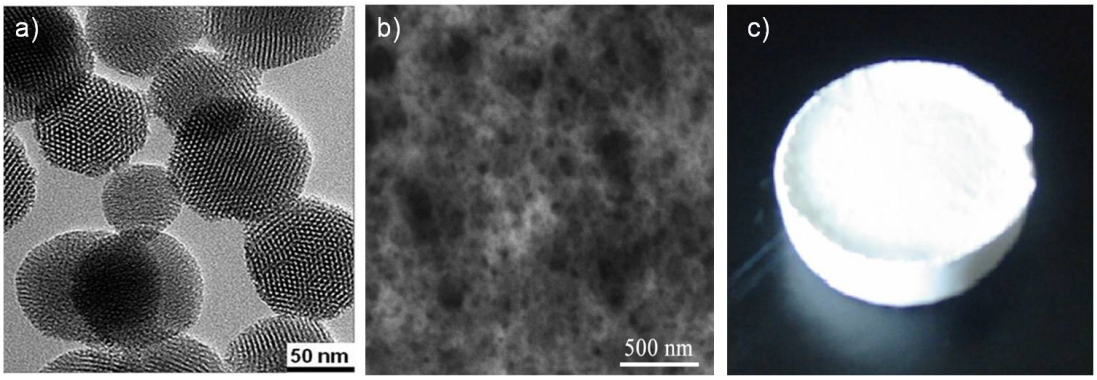

Figure 2.4: Different forms of mesoporous silica. (a) particles, (b) thin film and (c) aerogel.

through non-covalent interactions resulting in self-assembly which can occur in hexagonal rod, lamellar crystal and spherical micelle organizations. Simultaneously, covalent bonds are formed between inorganic Si blocks of the monomer via condensation reaction resulting in a liquid crystalline-surfactant composite. This process is known as cooperative assembly. On the other hand, a subsequent condensation reaction between Si atoms may occur around a pre-formed surfactant phase which is known as liquid crystal templating (LCT) mechanism. Mesoporous silica network is formed after surfactant removal by calcination or solvent extraction. The size and shape of the mesoporous silicas can be tuned; hexagonal, cubic and lamellar orderings can be obtained by changing surfactant type and surfactant concentration [41, 42].

2.2.2 Silica Aerogels: Template Free Prepared Mesoporous Silica Materials

Aerogels are a specific class of randomly porous materials with very low-density and high porosity up to approximately 90%. Aerogels can be prepared with a wide material classes ranging from inorganic oxides such as silica and titania to polymers. Among all the classes, silica based aerogels have gained the highest importance for their low refractive index, high transparency and low thermal

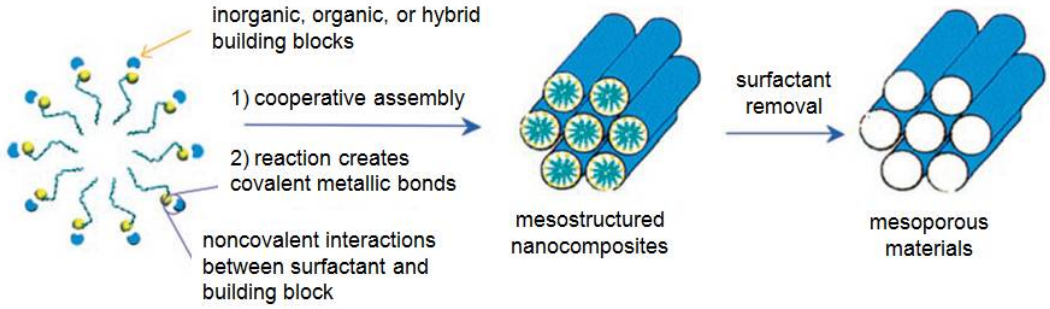

Figure 2.5: Template based synthesis of mesoporous silica from alkoxide monomers.

conductivity. In order to obtain a silica aerogel, firstly a wet silica gel is produced via the sol-gel process. Then the liquid in pores of the gel is removed through a supercritical drying process resulting in a low density porous gel called as aerogel. On the other hand, a xerogel is obtained with shrinked pores when the wet gel is dried at ambient conditions [43].

Aerogels were prepared by Kistler for the first time in 1931. He produced aerogels of silica, alumina, ferric oxide, cellulose by removing liquid from synthesized wet gels via supercritical drying [44, 45]. After his studies, supercritical drying method have been applied as the most efficient method for the aerogel preparation.

In the supercritical drying process, pressure and temperature of the container are increased over the critical pressure (P_c) and critical temperature (T_c) of the liquid in the container. Thus, the surface tension of liquid is decreased by converting it to a supercritical liquid and consequently the capillary pressure is avoided on the pore walls of the gel being dried resulting in highly porous gels.

In the ambient drying process, pore collapse occurs due to the high capillary force on the pores and gels become nonporous. Brinker and co-workers reported a novel method for the preparation of aerogels which possess 98.5% porosity despite the ambient drying conditions [46]. They added surface groups to the gel

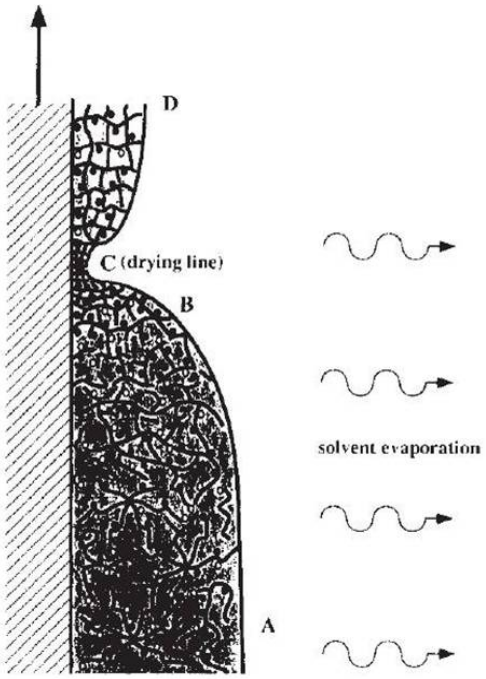

Figure 2.6: Stages of structural evolution of aerogel film during evaporation of liquid and spring-back effect.

network in order to prevent pore collapse during the ambient pressure drying. The structural changes in the pores during evaporation of the liquid is shown in Figure 2.6. In the region between A and B gelation occurs. The sol at this stage is highly concentrated and polymerization can continue. B-C region shows initial drying stage and pores of the gels shrink due to the capillary pressure created by evaporating liquid in this stage. C-D region shows complete removal of the liquid and in this stage, the sol exhibits spring-back behavior and expands to the original state because of organically functionalized surface [46].

2.2.3 Ormosils

Organically modified silicas (ormosils) are produced from organotrialkoxysilanes via the sol-gel reactions. Organotrialkoxysilanes having $RSi(OR)_3$ formula differ

from tetraalkoxysilanes ($Si(OR)_4$) by possessing a non-hydrolyzable functional (R) group substituted with an alkoxy (OR) group. A few examples of well known functional groups are methyl, ethyl, octyl, phenyl, aminopropyl, and mercaptopropyl [40]. Those alkyl groups give the gel different functional properties such as hydrophobicity, flexibility and mechanical stability. The condensation products of organotrialkoxysilanes are known as silsesquioxanes with the general formula $RSiO_{1.5}$ and polymers formed from interconnected silsesquioxane units are polysilsesquioxanes.

Alkyl groups, solvent polarity, pH and temperature affect gel structure and macro-meso porosity. Since most of the alkyl groups are intrinsically hydrophobic, they cause phase separation in polar solvent media resulting in a heterogeneous distribution of condensates. In addition, hydrolysis and condensation reactions become slower due to phase separation. Reactivity of the alkyl groups also affects the homogeneity of the gel. Trialkoxysilanes with small substitutes such as methyl form more homogenous gels compared to those with larger alkyl groups such as vinyl or phenyl [40].

In recent years there has been great attention on ormosils for the preparation of functional surfaces since ormosils offer mild, cost-effective synthesis and coating conditions. The properties which can not be achieved by glasses and polymers alone can be obtained with ormosils in one material. Ormosils can possess the mechanical and thermal stability of inorganic (silica) groups besides functionality and flexibility of organic groups. Furthermore, the chemical and physical properties of ormosils can be tailored accordingly with the targeted application. In Figure 2.7 examples of functional surfaces prepared from ormosils are shown [47, 48]. In these studies, superhydrophobic and highly transparent ormosil coatings were prepared on glass and various flexible substrates.

Ormosils can interact with doped molecules via noncovalent interactions. This property of ormosils permits to the physical entrapment of fluorophores and nanoparticles in ormosil matrices. Noncovalent interaction types are ionic, hydrophobic interactions, hydrogen bonding and nanoconfinement. Ionic interactions occur between cations and $Si\text{-}O^-$ sites of ormosils. Hydrogen bonding occurs

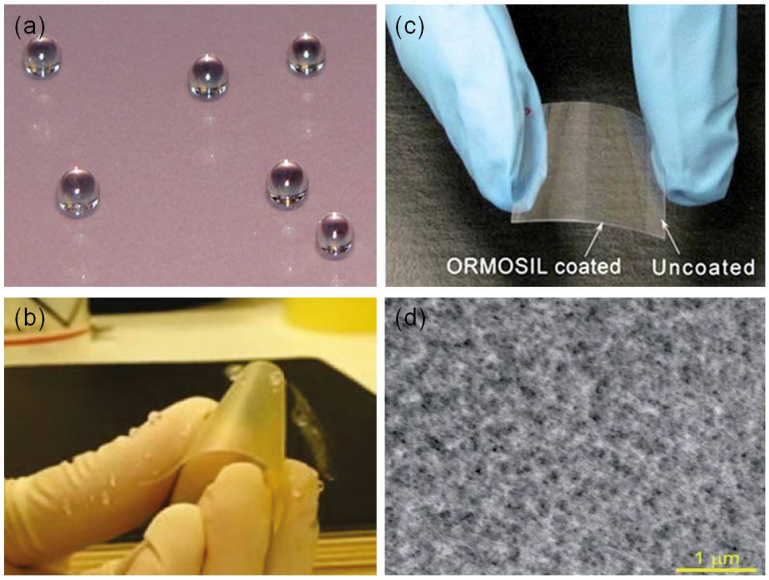

Figure 2.7: Functional surfaces prepared from ormosil. Photographs of (a) superhydrophobic film on glass with a water contact angle 178.4° (b) superhydrophobic film on flexible substrate, (c) transparent film on flexible substrate and (d) SEM image of porous ormosil film.

between dopants and silanols (Si-OH). Hydrophobic interactions occur between hydrophobic dopants and organic groups of ormosil. Nanoconfinement effect on the doped molecules is originated from the steric restraints in porous silica matrix [49].

2.3 Pyrene Excimer Formation in Thin Films

Pyrene is a fluorescent, polycyclic aromatic hydrocarbon compound. It has been an attractive sensing and probing molecule for an expanded range of application since it has long lifetime and high quantum efficiency. When two pyrene molecules interact via π-π^* stacking which is a non-covalent interaction occurring between aromatic molecules, an excimer forms. Pyrene excimers demonstrate high sensitivity to microenvironmental changes [1].

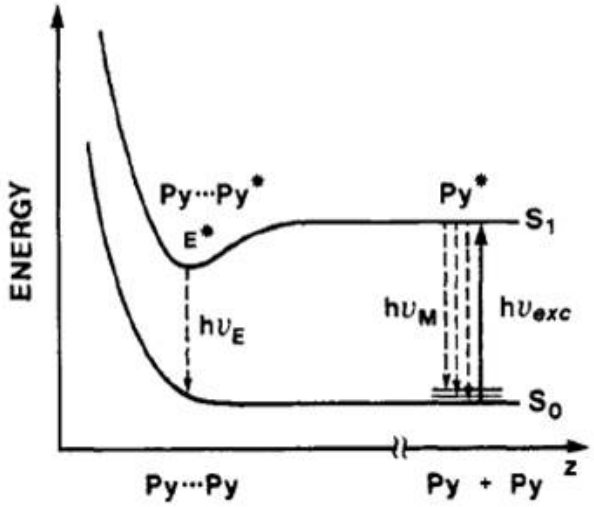

Figure 2.8: Potential energy diagram for pyrene excimer formation.

Molecular fluorescence spectrum of pyrene consists of different vibration bands which correspond to the radiative transitions from the first π electronic excited singlet state S_1 to different vibration levels of the ground singlet state S_0 (Figure 2.8) [3]. When pyrene forms excimer, a fluorescence band at lower energies than the fluorescence of singlet excited pyrene (monomer) originates.

Figure 2.9 shows the fluorescence spectrum of pyrene. The fluorescence of a singlet excited pyrene molecule shown in (2.1) is observed at 374, 384 and 394 nm in the spectrum. (M^* is singlet excited molecule, M: unexcited molecule)

$$M^* \longrightarrow M + h\upsilon_M \tag{2.1}$$

The interaction of the singlet excited pyrene with an unexcited pyrene yields an excited dimer (D^*) as depicted in (2.2).

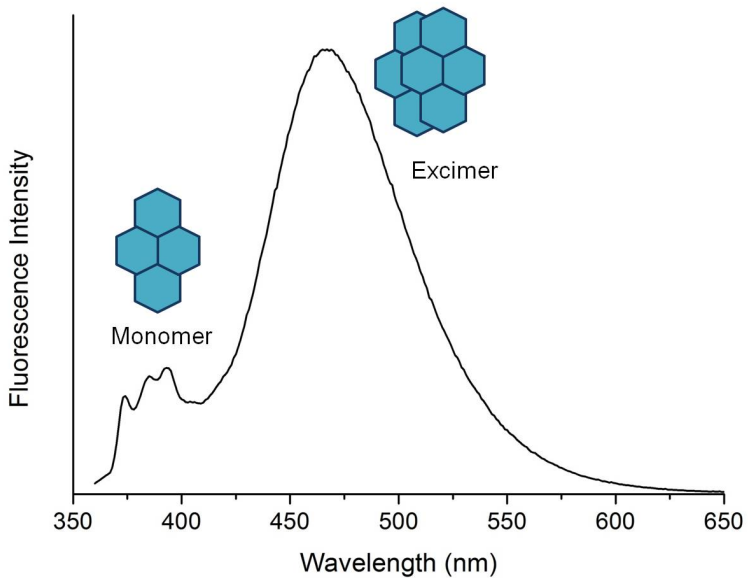

Figure 2.9: Fluorescence spectrum of pyrene showing the monomer and excimer emission of pyrene molecules.

$$M^* + M \longrightarrow D^* \tag{2.2}$$

The relaxation of the excited dimer radiates light as depicted in (2.3) at a broad wavelength range centered around 470 nm [3, 50].

$$D^* \longrightarrow M + M + h\upsilon_D \tag{2.3}$$

Pyrene excimers give fluorescence response to the molecular changes [1, 2]. For example, pyrene excimers are applied as probe molecules for the examining structural changes in nucleotides of DNA. Pyrene functionalized probe nucleotides are prepared by replacing pyrene with nucleobase or attaching pyrene to nucleobase or sugar moieties of DNA fragments [51]. An example probing mechanism

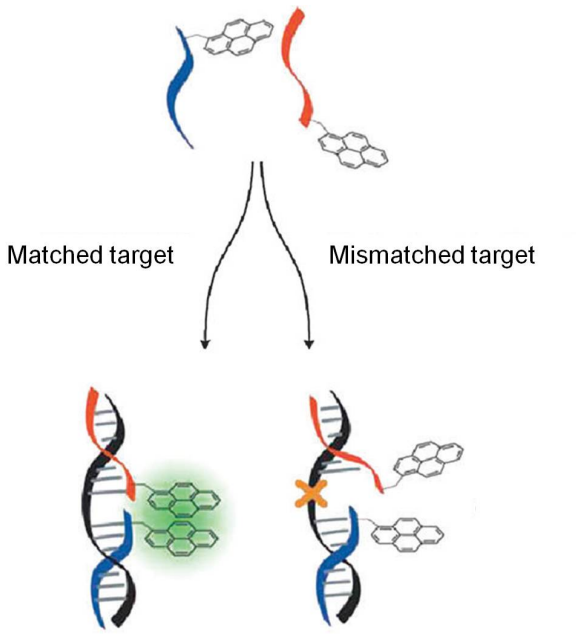

Figure 2.10: Schematic of probing DNA strand matches by pyrene functionalized DNA fragment.

by pyrene functionalized DNA fragments is shown in Figure 2.10. In this study, probe exhibits excimer emission upon hybridization of DNA strand with complementary DNA. On the other hand, probe does not exhibit excimer emission with mismatched DNA since pyrene molecules in the probe DNA and target DNA can not encounter and form excimer [52].

Pyrene is encapsulated in thin films or covalently attached to surfaces which are prepared for nitroaromatic explosives sensing [12, 53, 54]. As pyrene excimers can interact with nitroaromatic explosives via π-π^* stacking and give electron to the electron deficient nitroaromatic explosives such as trinitrotoluene (TNT), fluorescence of pyrene excimer is quenched in the presence of nitroaromatics. Figure 2.11a shows scanning electron microscope (SEM) image of a pyrene doped polystyrene fiber based thin film. In this study, fluorescence of pyrene excimer is quenched against dinitrotoluene (DNT) vapor (Figure 2.11b) [11].

Pyrene excimer formation is a prerequirement for all visible fluorescence based

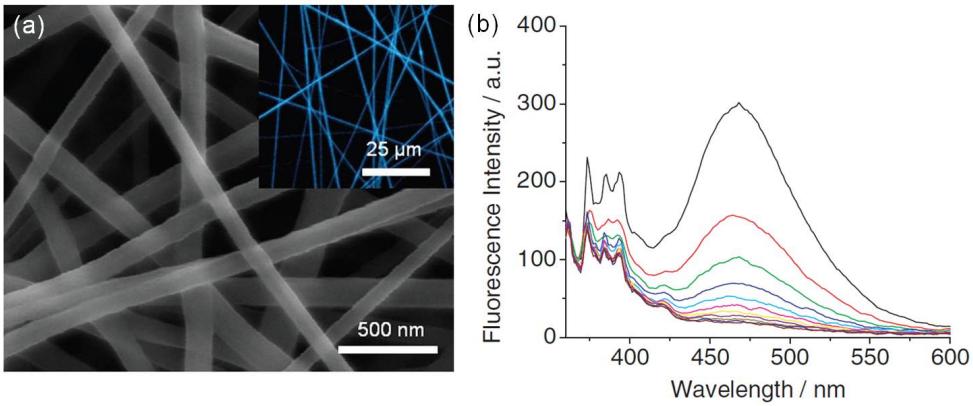

Figure 2.11: (a) SEM image of pyrene doped polystyrene fiber based thin film. (b) Fluorescence quenching response of the film to DNT molecule.

probing and sensing applications. In order to form pyrene excimer, an electronically excited pyrene must interact with ground state pyrene at an intermolecular distance less than 1 nm [3, 50]. Furthermore, pyrene excimers with excimer emission are promoted to form at high concentrations. On the other hand, only monomer emission occurs at low concentrations. Pyrene excimer formation is controlled by diffusion in solution phase, whereas it is controlled by the chemical and physical structure of its environment in thin films where diffusion is very slow [13].

Physical encapsulation is applied by mixing pyrene with thin film depositing solution of polymers such as polystyrene which is structurally similar with pyrene. Pyrene can be simply trapped in the polystyrene environment via π-π^* stacking interaction with phenyl groups of polystyrene. Pyrene can also be trapped within a sol-gel derived silica matrix by dissolving in the gel synthesis solution. A silica aerogel monolith doped with a pyrene derivative is shown in Figure 2.12 [5]. Fluorescence of the encapsulated pyrene in the silica aerogel monolith can be clearly observed under UV light. Pyrene can also be covalently attached to substrates via self-assembled monolayer (SAM) approach [53, 54].

Figure 2.12: Photographs of a pure silica aerogel monolith (left) and of a silica aerogel monolith doped with pyrene derivative (right) under UV light.

2.4 Explosive Detection Methods

Identification and quantitative analysis of explosives have been an important concern due to the security threats. Trace, surface and vapor explosive detecting instrumentation and methods have been developed for screening people, packages, luggage and vehicles.

Fixed or portable instrumentation are used to detect explosives. Detection speed, sensitivity and selectivity are considered properties in the design of the instruments. In addition, cost efficiency, reliability and portability are significant parameters for explosive sensors. As an effective method, canines are trained on specific explosive molecules and used for the detection of explosives since they have extremely sensitive nose. Although using canines is very efficient, there are some problems related to training them such as high training cost and decreasing performance due to behavioral changes in these animals [55, 56].

2.4.1 Properties of Explosives

Explosive is a material containing very unstable molecules which lead very fast reaction rates, large amount of heat and gaseous generation. Explosive reactions

are initiated by shock or heat which results in a rapid expansion and very fast decomposition in the material. Most of the explosives contain nitrogen and oxygen; in a less extent, carbon and hydrogen [55, 56].

Explosives are divided into two main classes as low and high explosives. Low explosives decompose at low rates (cm s^{-1}) without forming shock whereas high explosives lead huge shock with velocities varying from 1 to 9 km s^{-1}. High explosives are separated into two groups as primary and secondary explosives according to their properties and functions. Primary explosives (e.g. peroxide based) are the types which are more susceptible to heat, friction. Their handling is very difficult due to their fast initiation. Secondary explosives include nitroaromatics (e.g. TNT), nitramines (Tetranitro-N-Methylaniline) and nitrate esters (e.g. nitroglycerine). Secondary explosives are usually used by military sites [57].

Detection methods vary depending on the property of the explosives. For instance, vapor phase methods depend on vapor pressure of the explosives. Vapor pressures and boiling points of some explosives are shown in Table 2.1. Some of the explosives such as nitromethane and trinitrotoluene (TNT) have very high vapor pressures, which enable vapor phase techniques applicable. On the other hand, vapor techniques are difficult to apply for low vapor pressure explosives such as tetryl and picric acid. Vapors of explosives are further prevented due to packaging of the explosives using special materials which make the detection extremely difficult. Detection of explosive particles adhered on surfaces are more efficient for low vapor pressure explosives since their traces do not disappear quickly from the exterior of packaging [55].

2.4.2 Common Explosive Detection Methods

Detection of explosives is generally performed by using metal detectors and instrumental analysis techniques. However, using metal detectors is unsuitable in the case of plastic packaging of explosives. Instrumental techniques include mass spectroscopy (MS), gas chromatography with mass spectroscopy (GC)-MS, infrared spectroscopy (IR) and Raman spectroscopy [58].

Table 2.1: Vapor pressures and boiling points of some explosives.

Explosive	Boiling Point (°C)	Vapor Pressure at 20°C (Torr)
Nitromethane	100	2.8×10^{-1}
2,4,6 Trinitrotoluene (TNT)	240 (explodes)	1.1×10^{-6}
Ethylene glycol dinitrate (EGDN)	114 (explodes)	2.8×10^{-2}
Tetranitro-N-Methylaniline (Tetryl)	187 (decomposes)	5.7×10^{-9}
Ammonium nitrate	210 (decomposes)	5.0×10^{-6}
Picric Acid (2,4,6 trinitrophenol)	300	5.8×10^{-9}

Among the instrumental techniques, mass spectroscopy has been the leading method in sensitive and selective explosive sensing. Ion mobility mass spectrometry (IMS) is the most widely used method since it can be integrated with a portable device. IMS is used in airports and its sensitivity is in the range of nanogram, however, it is an expensive method [55, 56].

Raman spectroscopy has been showed to detect explosives at stand-off distances and portable Raman instruments have been designed for field use. Fluorescence interferences and weak Raman signals are the major problems with Raman Spectroscopy. Surface Enhanced Raman Spectroscopy (SERS) is developed to increase the Raman intensity and sensitivity by using metal nanostructures [55]. In Figure 2.13a, an example SERS paper prepared with gold nanorods and TNT binding peptides is shown. In this study, gold nanorods were prepared in order to enhance Raman signals and sensitivity of the sensor paper for TNT. It is shown that strong Raman signals can be observed with 10 µg TNT by using the prepared SERS paper (Figure 2.13b) [59]. However, poor selectivity and lack of facile methods to produce SERS substrates for field use are two major problems with SERS.

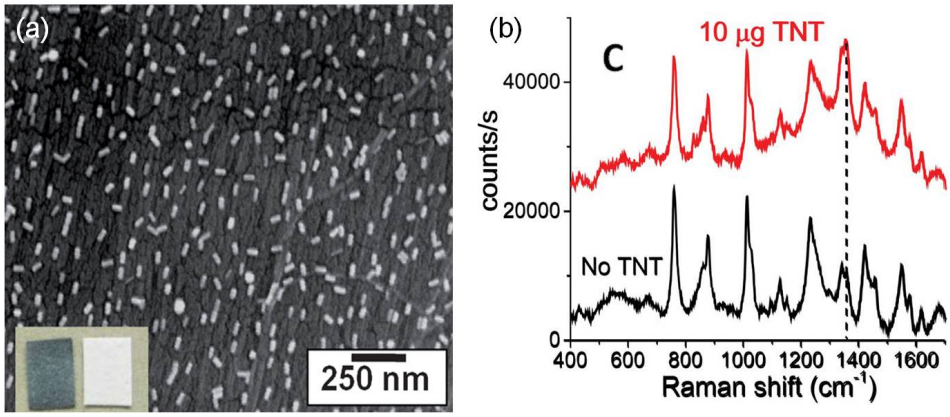

Figure 2.13: (a) SEM image of a SERS substrate prepared for the detection of TNT. Inset shows the photographs of SERS paper (left) and bare paper (right)(b) Raman signal before and after SERS paper was exposed to TNT.

2.4.3 Fluorescence Quenching Based Explosive Detection Methods

Although GC-MS methods are sensitive and selective, they are expensive. Therefore, low-cost and facile devices and methods are required for the detection of explosives. Nitroaromatic explosives constitute a significant part of explosives and since they can interact with electron donating fluorescent molecules, they can be detected via fluorescent quenching based method. [60].

Nitro groups withdraw electron making the nitroaromatic molecules good electron acceptors. On the other hand, delocalized π^* excited states in the fluorescent dyes and fluorescent conjugated polymers make them good electron donors and facilitates electron-transfer fluorescence quenching. Fluorescence and fluorescence quenching mechanism of a fluorescent molecule in the absence and in the presence of a nitroaromatic molecule is shown in Figure 2.14. In the absence of nitroaromatic molecule, excited electron relaxes back to the ground state by emitting light. In the presence of nitroaromatic molecule, the excited electron is transferred from the electron donor fluorescent molecule to the LUMO of the nitroaromatic molecule instead of relaxing back to the ground state [60]. Therefore, fluorescence intensity of the electron donor is quenched in the presence of a

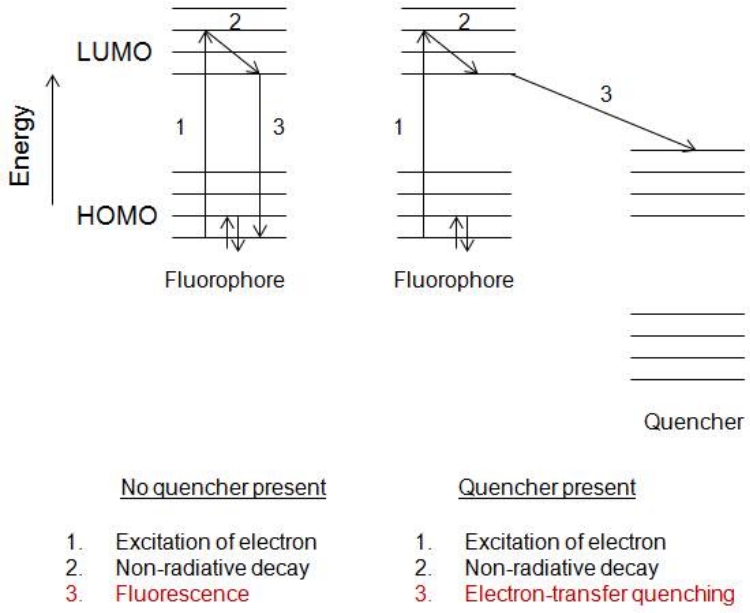

Figure 2.14: Mechanisms of fluorescence and electron transfer fluorescence quenching of an electron donor molecule.

nitroaromatic molecule.

As the number of nitro groups increases, redox potential of nitroexplosive increases. Redox potentials of nitrobenzene (NB), dinitrotoluene (DNT) and trinitrotoluene (TNT) are -1.15 V, -1.0 V and -0.7 V, respectively indicating that TNT is better electron acceptor compared to DNT and NB. However, since DNT and NB have higher vapor pressure than TNT, they can more highly quench fluorescence of sensing molecules compared to TNT [60].

Fluorescent conjugated polymers are commonly prepared as nitroaromatic explosive sensing materials since they respond with amplified signals and high sensitivity in parts per million (ppm) and parts per billion (ppb) levels. Conjugated polymers have increased delocalization in their π^* excited states, which allows efficient exciton migration. Signal amplification in conjugated polymers is enabled by efficient exciton migration. Thin films of conjugated polymers with thickness less than 10 nm are more efficient than those with thickness higher

than 20 nm due to increased diffusion rate of explosive vapors within the thinner polymer structure [58].

Fluorescent, polycyclic aromatic hydrocarbons (PAHs) such as pyrene and anthracene can be used as nitroaromatic explosive sensing molecules by physically encapsulating in matrices or covalently binding to surfaces [11, 12, 53, 54]. These molecules with their π^* conjugated molecule structure can interact with nitroaromatic explosives which provides fast fluorescence quenching response [61].

Porphyrin and its derivatives are electron donating fluorescent dyes and they are doped in silica, polystyrene fibers; physically or covalently incorporated in mesoporous silica thin films for nitroaromatic molecule sensing applications. Fluorescence of porphyrin is quenched against explosives such as TNT and DNT due to high affinity of porphyrin for nitroaromatics via hydrogen bonding and π-π^* stacking interaction. In several studies, it is shown that porphyrin doped fluorescent films can be prepared by using simple methods and fluorescence of porphyrin can be quenched against TNT via the electron transfer quenching mechanism (Figure 2.15) [18, 62, 63, 64, 65].

Pyrene among the fluorescent molecules has very advantageous with its high quantum efficiency, long lifetime and high sensitivity to its micro-environment. For example, pyrene gives faster response to nitroaromatic explosives compared to porphyrin because of its similar structure to nitroaromatics and its π-π^* stacking interaction with nitroaromatics. Furthermore, fluorescence quenching of pyrene in the presence of nitroaromatics can be visually observed under UV-light illumination.

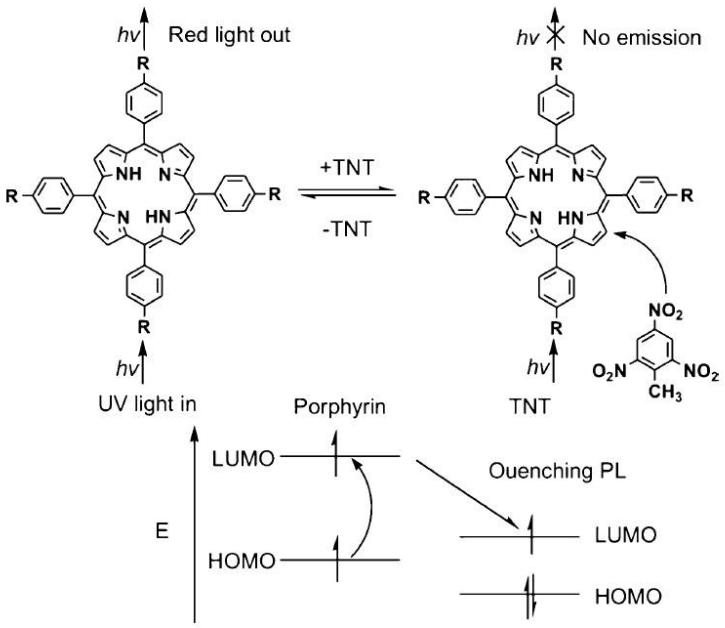

Figure 2.15: Schematic for electron transfer quenching of porphyrin fluorescence by TNT.

Chapter 3

Experimental

3.1 Materials

Methyltrimethoxysilane (MTMS), dimethylsulphoxide (DMSO), methanol, oxalic acid and ammonium hydroxide (25%) were purchased from Merck (Germany). Ethanol, hydrochloric acid (37%) and pyrene were purchased from Sigma-Aldrich. All chemicals were used as received without any purification.

3.2 Characterization

3.2.1 Transmission Electron Microscopy (TEM)

Transmission Electron Microscope (Tecnai G2-F30, FEI) operated at 200 kV was used to investigate the structure of ormosil colloids. TEM samples were prepared on a holey carbon coated copper grid by placing a 2 µL of colloidal ormosil suspension used for film preparation.

3.2.2 Scanning Electron Microscopy (SEM)

Scanning Electron Microscope (E-SEM, Quanta 200F, FEI) was used to carry out the microstructural observations of the thin films at 10 kV, under high vacuum condition. 7 nm thick gold-palladium layer was coated on the films before placing the films in the microscope.

3.2.3 Atomic Force Microscopy (AFM)

Atomic Force Microscope (XE-100E, PSIA) was used in non-contact mode to analyze the surface morphology of the films.

3.2.4 X-Ray Photoelectron Spectroscopy (XPS)

X-ray Photoelectron Spectroscopy (K-Alpha, Thermo Scientific) was used to perform the chemical analysis of the films coated on silicon substrates. XPS measurements were performed after surfaces of the films were slightly etched by ion gun. The data was collected at survey mode and flood gun was operated in order to prevent charging of the surfaces.

3.2.5 UV-Visible Spectroscopy

UV-Vis Spectrophotometer (Cary 100, Varian) was used to record the absorption spectrum of the pyrene doped colloidal ormosil solution. UV-Vis spectra were recorded between 200 and 800 nm in absorption mode.

3.2.6 Fluorescence Spectroscopy

Fluorescence Spectrophotometer (Varian Eclipse) was used to record the fluorescence spectra of the films. The spectrum was recorded between 360 and 650 nm

with excitation at 340 nm in emission mode. Thin films were placed on a holder at an angle of 45°.

3.2.7 Ellipsometric Measurements

Ellipsometer (V-Vase, J. A. Woollam) was used to measure thickness and refractive indices of the films. The measurements are performed in the 400 to 1000 nm range. The experimental results were fitted; thickness and refractive index values were calculated by using Cauchy model as given in Eq. (3.1).

$$n(\lambda) = A + \frac{B}{\lambda^2} + \frac{C}{\lambda^4} \tag{3.1}$$

where, n is refractive index, A (dimensionless), B (μm^2) and C (μm^4) are Cauchy parameters.

3.2.8 Contact Angle Measurement System

A contact angle meter (OCA 30, Dataphysics) was used to measure the static water contact angles of the prepared surfaces. For measurments, water droplets of 4 µL volume were dispensed onto film and Laplace-Young fitting was applied on the measurement.

3.3 Preparation of Pyrene Doped Mesoporous Ormosil Thin Films

Ormosil thin films were prepared by modifying the previous methods [36, 37, 47, 48]. Ormosil gel was first prepared via two-step sol-gel reaction. First, 1 mL of MTMS was added to the mixture of 4.88 mL of methanol and 3.88 mL of

DMSO. Different amounts of pyrene was dissolved in 1 mL of DMSO and added to MTMS solutions. For example, 20 mg of pyrene was used to prepare films containing 4.14 mM pyrene. Then, 500 µL of 1.0 mM aqueous oxalic acid solution was added dropwise to start the hydrolysis of monomer. Synthesis solution was stirred for 30 minutes and then was left to hydrolyze completely for 24 hours at room temperature. After hydrolysis step, 0.42 mL of ammonium hydroxide (25%) solution and 0.19 mL of deionized water were added to the solution and it was stirred for further 15 minutes. Finally, solution was poured into a polystyrene vial and left for gelation at 25 °C. The gel was aged at this temperature for 48 hours in order to strengthen the porous network. After aging, different amounts of methanol were added onto gel to adjust the film thickness and gel was sonicated by an ultrasonic liquid homogenizer at 20 W for 45 seconds. For example, for 251 nm thick film 12 mL of methanol was added to the gel as diluting solvent. Finally, an ormosil sol which is suitable for thin film deposition was obtained. Glass substrates with 2 cm x 1 cm dimensions were cut, then cleaned in ethanol and isopropanol mixture and finally dried. 250 µL portions of the ormosil sol were dispensed onto glass substrates and were coated by using a spin-coater at 3000 rpm for 45 seconds. Porous thin films were left to dry at room temperature.

3.4 Preparation of Pyrene Doped Nonporous Ormosil Films

We prepared the nonporous films by slightly modifying our previous method [36]. First, 2.25 mL of MTMS was dissolved in 1.12 mL of ethanol. 20 mg of pyrene was dissolved in 1.12 mL of DMSO. Then, pyrene solution, 0.2 mL of deionized water and 5 µL of 0.1 M hydrochloric acid were added under gentle stirring. Synthesis solution was stirred at 60 °C for 90 minutes. After that, 0.4 mL of 0.1 M hydrochloric acid and 0.35 mL of deionized water were added and solution was further stirred at ambient temperature for 15 minutes. Finally, sol was left for aging at 50 °C for 15 minutes. 2 mL of the aged sol was diluted with 0.4 mL of methanol in order to adjust film thickness around 275 nm. 250 µL portions of

the sol were dispensed onto previously cleaned glass substrates and were coated by using spin-coater at 3000 rpm for 45 seconds. Nonporous ormosil thin films were left to dry at room temperature.

3.5 Nitroaromatic Explosive Sensing Experiments

Approximately 10 mg of TNT was put inside a 15 mL vial and then, a piece of cotton was placed onto top in order to prevent direct contact of film with TNT. Vial was kept closed at least for 2 days prior to sensing experiments in order to assure that TNT vapor reached equilibrium. Before exposing of porous film to TNT vapor, emission of the film was recorded using fluorescence spectrophotometer. Then, film was placed onto the cotton piece in the vial and kept closed for a specific time. After that the film was taken out of the vial and its emission was recorded again. Samples of DNT, benzoic acid, ammonium nitrate and 3,4 dihydroxybenzoic acid (3,4 DHBA) were prepared similarly as done with TNT and were kept in closed vials at least for 2 days prior to sensing experiments. Samples of toluene, methanol, nitrobenzene, benzene and sodium hydroxide were prepared by wetting a piece of cotton with a small amount of liquid analyte, then, wetted cotton was kept in closed vial. Sensing experiments were performed with all other analytes similarly as done with TNT.

Chapter 4

Results And Discussion

4.1 Preparation and Characterization of Pyrene Doped Ormosil Thin Films

In the scope of this thesis, we investigated the formation of pyrene excimers in ormosil thin films and showed the application of those films for nitroaromatic explosive sensing. In the first step, we prepared ormosil gels by using MTMS monomer via a template-free sol-gel method. We dissolved the pyrene molecules in DMSO and added to the starting reaction solution to obtain a final dye concentration of 4.14 mM. We did not use any covalent binding agents for immobilizing pyrene dye in the gel in order to eliminate tedious synthesis steps. During gelation, pyrene molecules are physically encapsulated in the porous ormosil network. The pyrene doped gel shown in Figure 4.1 (right) is homogenously fluorescent revealing the successful encapsulation of pyrene. On the other hand, gel shown in Figure 4.1 (left) which was prepared without adding pyrene has no fluorescence. In the second step, we broke down the gel network by ultra-sonication in order to obtain ormosil sols which are suitable for thin film deposition. In the final step, we coated the ormosil sols onto glass substrates via spin-coating method. In order to evaluate the effect of porosity on the formation and stability of pyrene excimers, we also prepared nonporous ormosil thin films by using the same monomer and

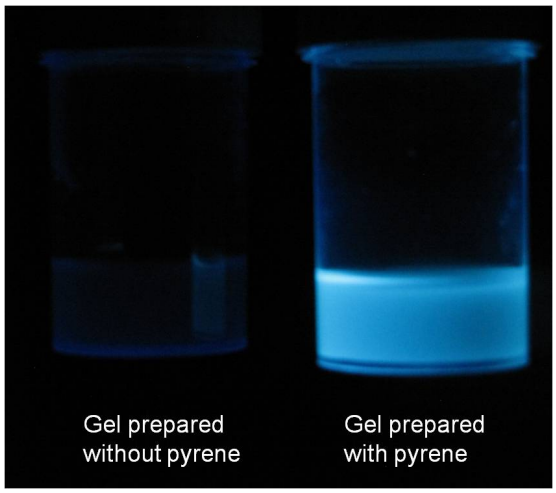

Figure 4.1: Photographs of the ormosil gels prepared with (right) and without (left) pyrene under UV light illumination. Gel without pyrene has no emission whereas the gel with pyrene has a very bright blue emission.

pyrene composition.

The porous and skeletal structure of pyrene doped ormosil colloids was investigated using a transmission electron microcopy (TEM). The TEM image in Figure 4.2 reveals the mesoporous network which is formed from the interconnected ormosil particles with diameter size of approximately 15 nm.

Surface morphology of the pyrene doped mesoporous ormosil film was investigated using a scanning electron microscope (SEM). Figure 4.3 shows the SEM image of 4.14 mM pyrene doped approximately 100 nm thick-ormosil thin film indicating uniform surface coverage and highly mesoporous film structure.

Surface of an approximately 1200 nm thick-film prepared with 4.14 mM pyrene was investigated by using an SEM Figure 4.4(a). SEM image of that film indicates more dense and compact film formation compared to the 100 nm thick-film due to the high ormosil concentration in the sol prepared for thick film coating. Furthermore, surfaces of approximately 250 nm thick-films prepared without pyrene and prepared with 0.52, 1.04, 2.07 and 8.29 mM pyrene were also investigated using an SEM. Images in the Figure 4.4(b-f) reveal that surface morphology and

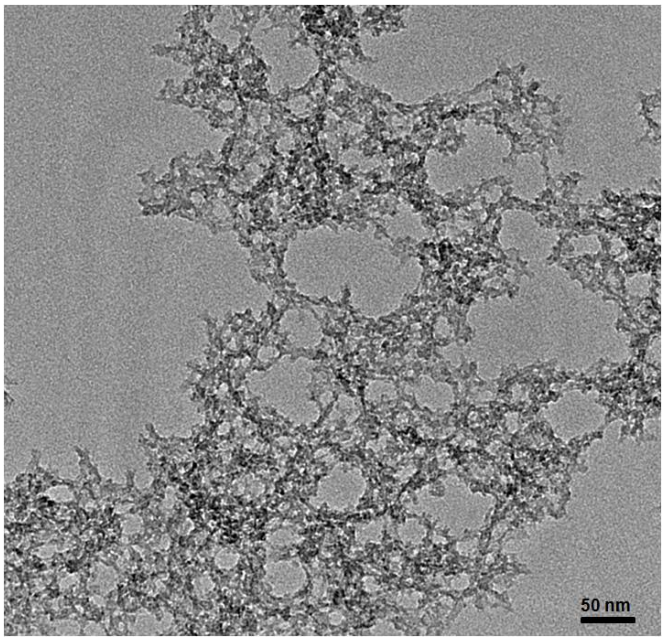

Figure 4.2: TEM image of the 4.14 mM pyrene doped ormosil.

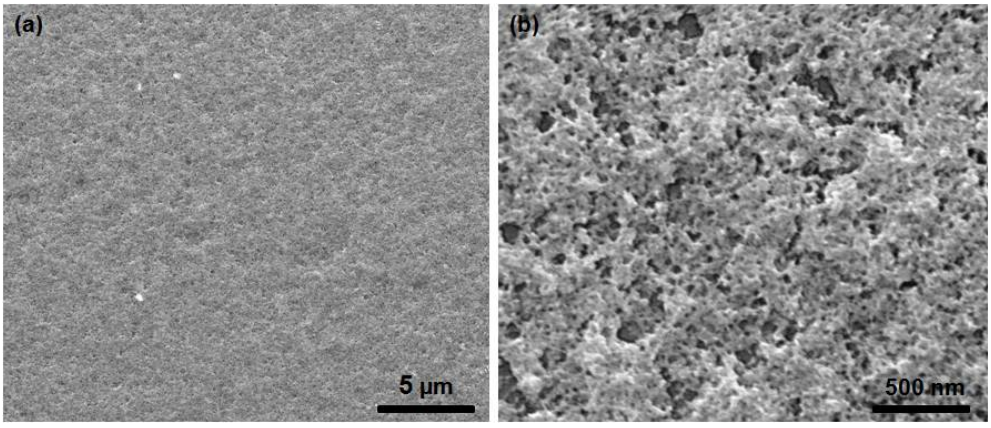

Figure 4.3: SEM images of 4.14 mM pyrene doped approximately 100 nm thick-mesoporous ormosil film. (a) Low magnification SEM image of the film. (b) Higher magnification SEM image of the same film.

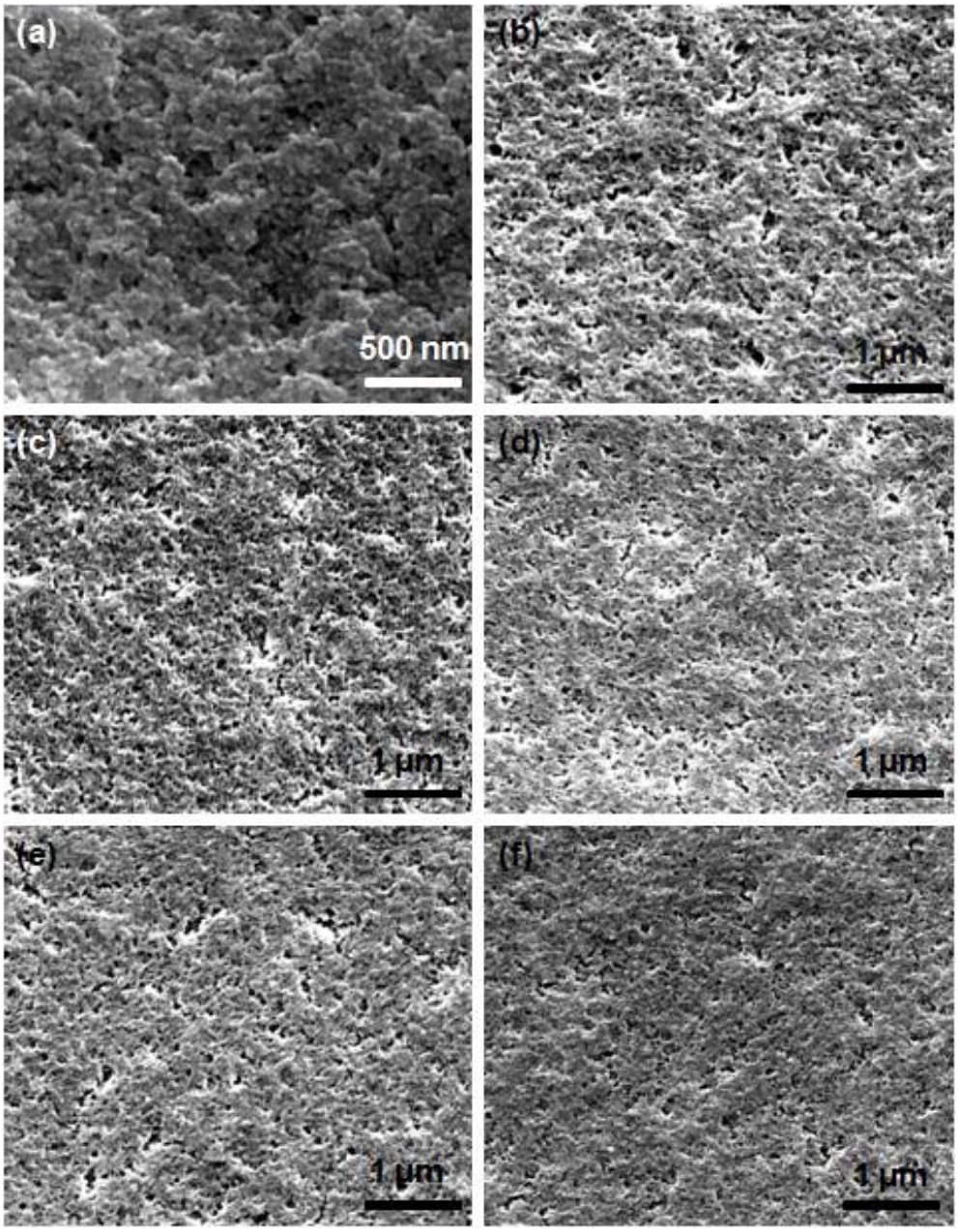

Figure 4.4: SEM images of (a) 1202 nm thick-film with 4.14 nM pyrene and 250 nm thick-films with (b) no pyrene (c) 0.52 mM pyrene (d) 1.04 mM pyrene (e) 2.07 mM pyrene and (f) 8.29 mM pyrene.

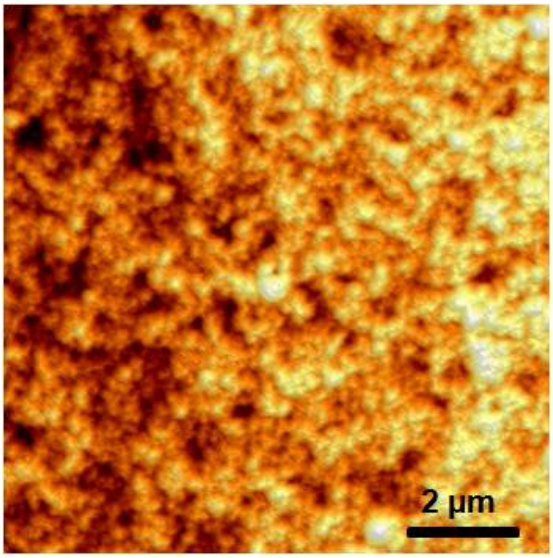

Figure 4.5: AFM image of the pyrene doped 100 nm thick-mesoporous ormosil film.

porous structure of the films are the same regardless from the varying pyrene concentration.

Surface morphology of the mesoporous ormosil film was also investigated by using atomic force microscope (AFM). The AFM image of a 4.14 mM pyrene doped approximately 100 nm thick-porous film shown in Figure 4.5 further reveals the porous film formation. We also investigated the morphology of the nonporous ormosil film with a thickness of approximately 275 nm using SEM and AFM methods. Both methods indicate nonporous, dense and smooth structure of the examined film (Figure 4.6).

Chemical analysis of the surface of 4.14 mM pyrene doped 250 nm thick-film was carried out by using X-ray photoelectron spectroscopy (XPS). Oxygen and silicon peaks in the spectrum shown in Figure 4.7 are originated from the inorganic part of the ormosil network. Carbon peak is originated from pyrene and methyl groups of the ormosil network. Oxygen, carbon and silicon contents are found to be 37.23%, 19.8% and 42.97%, respectively.

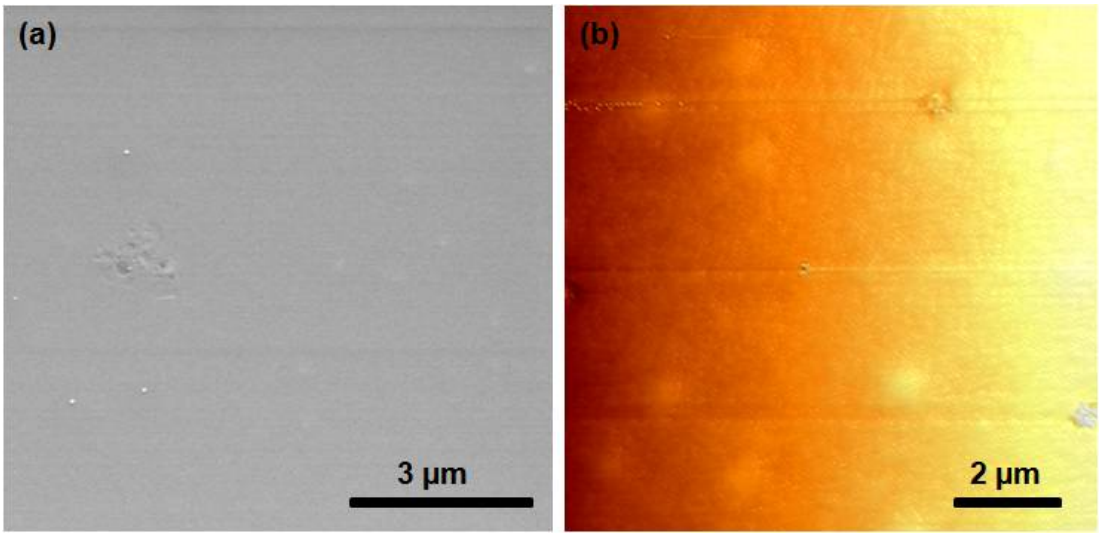

Figure 4.6: Surface morphology of the pyrene encapsulated 275 nm thick-nonporous film. (a) SEM image and (b) AFM image of the nonporous film.

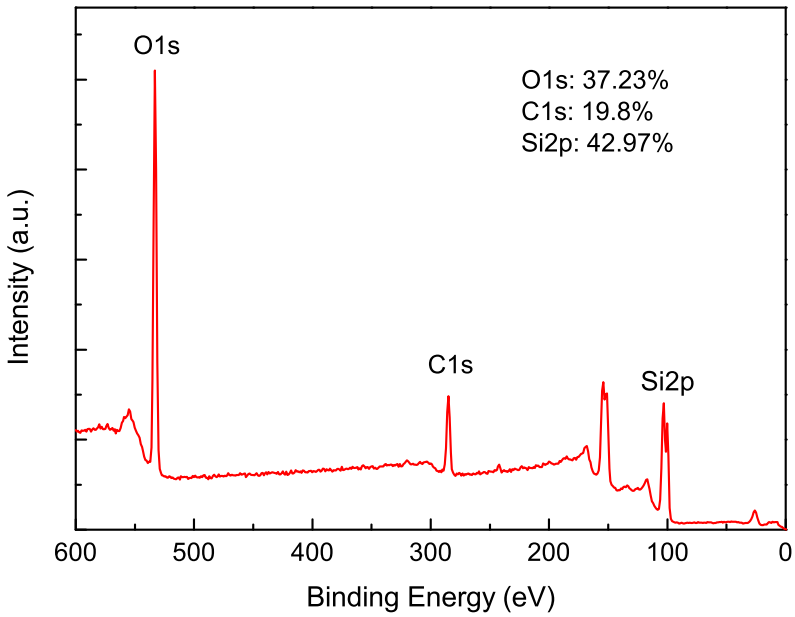

Figure 4.7: XPS spectrum of 250 nm thick-ormosil thin film containing 4.14 mM pyrene.

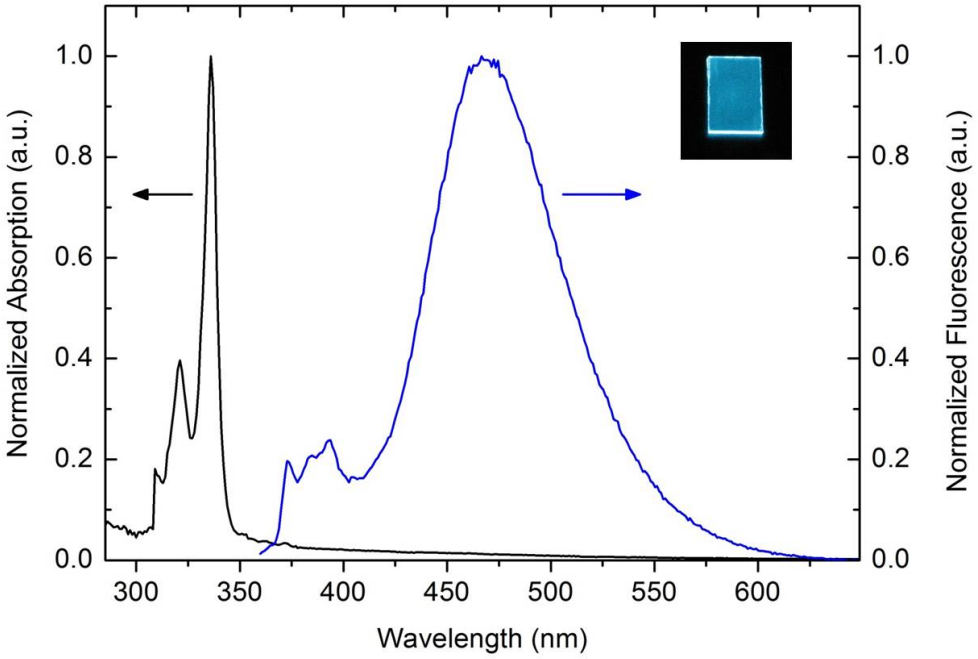

Figure 4.8: Normalized absorption spectrum (black) of pyrene doped ormosil colloid and normalized fluorescence spectrum (blue) of 4.14 mM pyrene doped 250 nm thick-ormosil thin film (Excitation wavelength is 340 nm). The inset shows the photograph of the thin film which was taken under UV light illumination.

Thicknesses and refractive indices of the films were measured using a spectroscopic ellipsometer. Refractive indices (at 600 nm) were measured as 1.166 and 1.42 for 251 nm porous and 275 nm nonporous films, respectively. Using the measured refractive indices of the films and Eq. (4.1) (n_p, $n_a$and n_d are the refractive indices of porous film, air and nonporous film, respectively), the porosity of the 251 nm porous ormosil thin film was calculated to be 60.5%.

$$Porosity = \left[\frac{n_d - n_p}{n_d - n_a}\right] \tag{4.1}$$

Absorption spectrum of pyrene in ormosil colloidal solution consists of a strong peak at 336 nm and a weaker peak at 321 nm, which are consistent with the

vibrational bands of pyrene (Figure 4.8) [3].

Two characteristic emission bands of pyrene were observed in the porous ormosil film (Figure 4.8). First main band is the monomer emission which consists of three individual peaks at 373, 385, 394 nm indicating the presence monomeric pyrene molecules. Second band is the excimer band with a fluorescence maximum at around 466-470 nm and corresponds to the formation of excimers through π-π^* stacking interaction of two pyrene molecules. Excimer emission of pyrene doped mesoporous ormosil film is very intense compared to monomer emission which is simply achieved by the physical encapsulation of pyrene excimers in the porous ormosil network. Also, the bright blue emission of pyrene excimers can be observed visually under UV light illumination (inset in Figure 4.8).

We prepared several 250 nm thick-porous ormosil thin films with different amounts of pyrene. Their fluorescence spectra are shown in Figure 4.9(a). As the pyrene concentration increases, both monomer and excimer emission intensities increase. A weak excimer emission for the film prepared using ormosil sol containing 0.52 mM pyrene is observed due to the lack of π-π^* stacking between pyrene molecules. When pyrene concentration is increased to 2.07 mM or above, a bright excimer emission can be observed. The concentration dependent enhancement of pyrene excimer emission can be attributed to the decreasing distance between pyrene molecules at higher concentration and consequently increasing π-π^* stacking possibility between pyrene molecules. We also calculated the ratios of excimer emission intensity to monomer emission intensity (I_{exc}/I_{mon}) for varying pyrene concentration. It is observed in Figure 4.9(b) that I_{exc}/I_{mon} ratio has an exponentially increasing behavior with respect to the pyrene concentration. The I_{exc}/I_{mon} ratio is 0.46 for the film containing 0.52 mM pyrene indicating poor excimer formation. On the other hand, it is 4.09 and 14.34 for the films containing 4.14 mM and 8.29 mM pyrene, respectively, demonstrating that most of the pyrene molecules formed excimers in these porous films. Accordingly, we determined an optimum pyrene concentration to be 4.14 mM in order to obtain bright excimer emission and we used this pyrene concentration in the rest of the study.

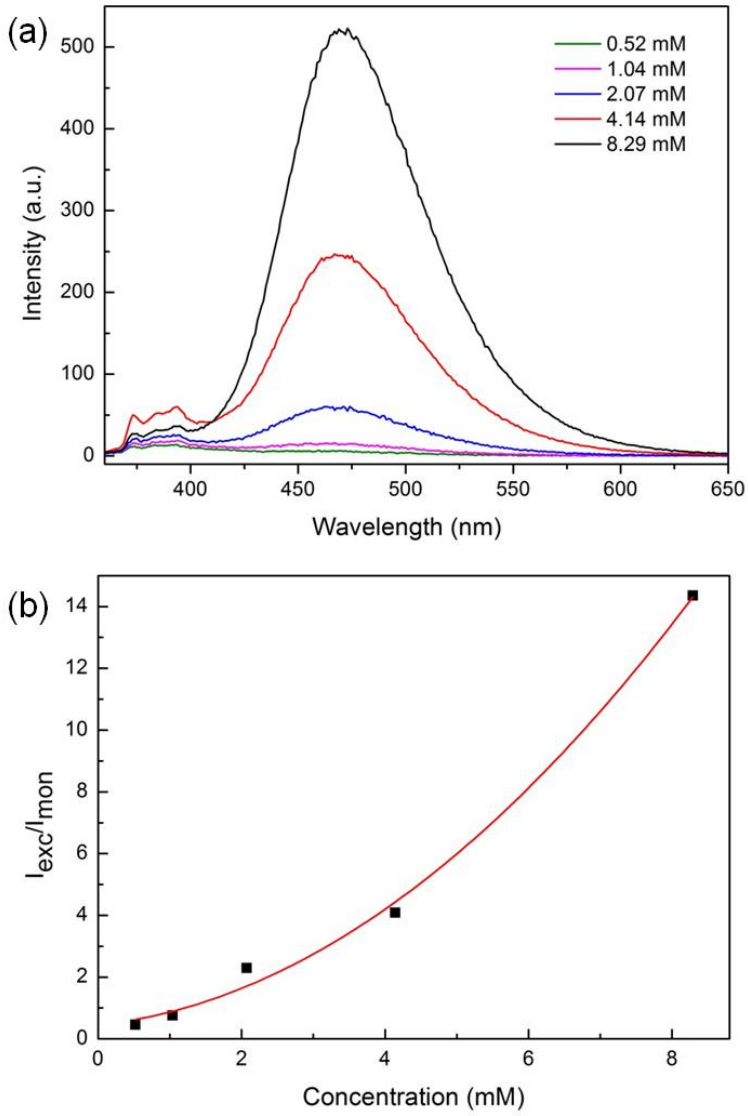

Figure 4.9: Effect of pyrene concentration on excimer emission intensity. (a)Fluorescence spectra of the films containing different amounts of pyrene. (b) Ratio of the excimer emission intensity to monomer emission intensity (I_{exc}/I_{mon}) with respect to pyrene concentration. (Intensities at 470 nm and 394 nm in the spectra given in (a) were considered for excimer emission and monomer emission, respectively).

4.2 Stability of Excimer Emission

Formation and emission intensity of pyrene excimers are strongly depended on the environment of the pyrene molecules. Excimer formation is controlled by diffusion in solution phase. However, excimers can aggregate in thin films which results in self-quenching and weak excimer fluorescence since solvent does not exist in thin films. There are ways which can be used to decelerate or eliminate aggregation. One way is the binding of molecules in the matrices or in the surfaces which prevent excimer aggregation due to steric hinderance. The other way is tuning the microstructure of the films. For example, mesoporous ormosil film structure with its randomly distributed organic groups in its nanoscale silica walls can be an efficient restriction environment to prevent the aggregation of pyrene molecules. Accordingly, we investigated the formation and stability of pyrene excimers in mesoporous ormosil thin films.

In order to evaluate the formation and stability of pyrene excimer emission, we monitored the emission intensities of porous and nonporous films at different time intervals. Figure 4.10 and Figure 4.11 show the emission spectra of pyrene doped mesoporous film and nonporous film, respectively. Porous ormosil film demonstrates a bright excimer emission with a high I_{exc}/I_{mon} ratio of 4.09. On the other hand, nonporous film has a significantly lower I_{exc}/I_{mon} ratio of 0.76. More importantly, the excimer emission intensity of the nonporous film almost completely quenched after 2 hours. Interestingly, the monomer emission of the nonporous film also quenched. This may be due to the increased aggregation of pyrene molecules during drying process, which self-quenches the emission of the monomer [50]. Porous ormosil film, on the other hand, revealed very slow decrease in the excimer emission compared to the nonporous film. Although the excimer emission of the porous film decreased gradually with time, it demonstrated very bright excimer emission even after one week. Figure 4.12 shows the change in the I_{exc}/I_{mon} ratio of porous and nonporous films with respect to time. As previously mentioned, I_{exc}/I_{mon} ratio of the nonporous film decreased rapidly and reached to a value around zero within a day indicating the complete quenching of the excimer emission. The I_{exc}/I_{mon} ratio of porous film decreased sharply from 4.09

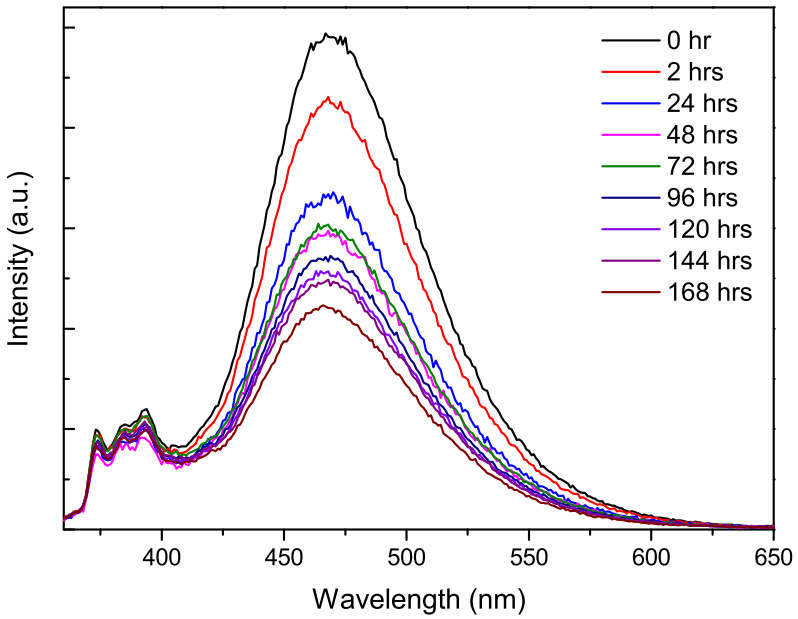

Figure 4.10: Fluorescence spectra of porous film with respect to time.

to 3.78 in the first 2 hours which may be due to the rapid solvent evaporation from the as-prepared films. After two hours, the decrease in the emission slowed down and reached a constant rate. Even after one week, a high I_{exc}/I_{mon} ratio of 2.21 was observed for the porous film.

It can be revealed that randomly distributed ormosil particles in the walls of the ormosil network largely prevents the aggregation of pyrenes and self-quenching of pyrenes and thus greatly improves excimer stability. It is important to note that time-dependent excimer stability of pyrene has not been investigated in most of the previous studies [13, 16, 17, 66, 67, 68]. Our results show the importance of investigation of excimer stability in order to produce thin films providing long-lived pyrene excimer emission.

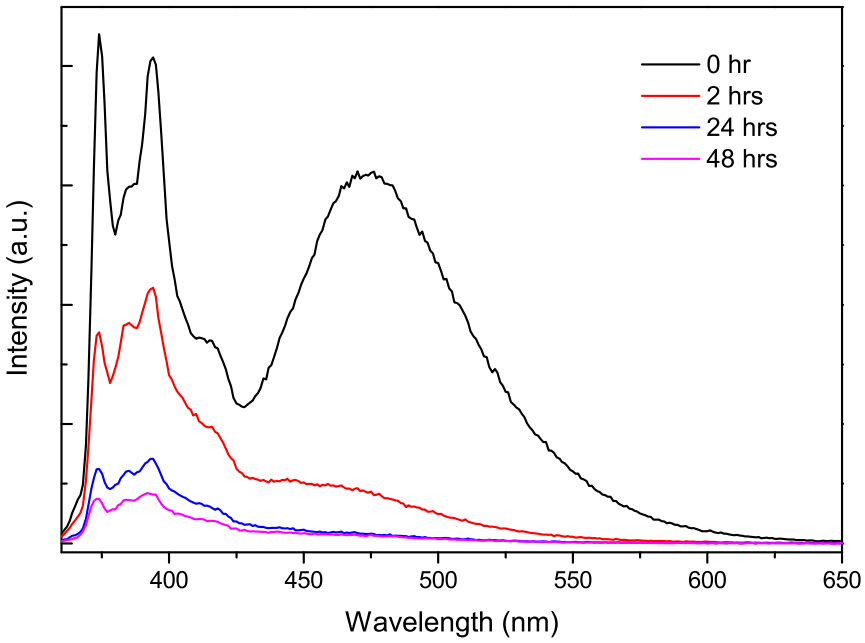

Figure 4.11: Fluorescence spectra of nonporous film with respect to time.

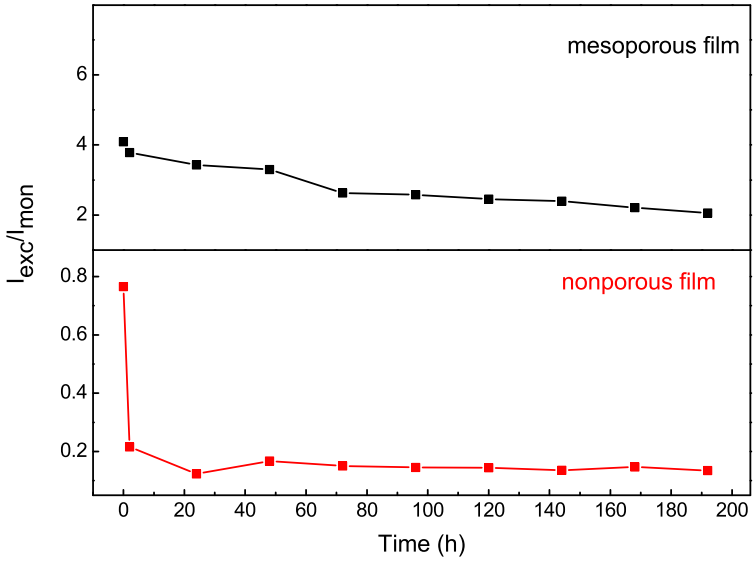

Figure 4.12: Change in the I_{exc}/I_{mon} ratios calculated by the values in the spectra given in Figure 4.10 and Figure 4.11 for porous and nonporous films, respectively. Porous film has significantly slower self-quenching and considerably higher I_{exc}/I_{mon} value compared to nonporous film.

Table 4.1: Physical properties of pyrene doped porous ormosil thin films used in nitroaromatic explosive sensing studies.

Film	Thickness (nm)	Refractive Index (n_D) at 600 nm	Porosity (%)	I_{exc}/I_{mon}
F1	108	1.112	73.3	1.21
F2	251	1.166	60.5	4.09
F3	1202	1.206	51	7.28

4.3 Nitroaromatic Explosive Sensing

Having very strong excimer emission and high porosity, our ormosil thin films are very promising for rapid detection of nitroaromatic explosives from their vapors. We evaluated TNT sensing performances of three 4.14 mM pyrene doped porous ormosil films with different thicknesses, which are given in Table 4.1. The thicknesses of the films were simply tuned by changing the concentration of the thin film deposition solution. For example, for thinner film preparation amount of methanol added to the gel was increased. Reduction in the porosity of the films with increasing thickness was observed due to the closer packing of the ormosil colloidal particles in more concentrated ormosil sol. Also, lower I_{exc}/I_{mon} ratio was observed for thinner films (Table 4.1) because of the decreasing pyrene concentration after diluting the ormosil sols.

Fluorescence quenching performances of the films were determined by keeping the films in a closed vial saturated with TNT vapor and measuring their fluorescence intensities after certain time intervals. Fluorescence quenching of F1 film against TNT is shown in Figure 4.13. We observed a rapid fluorescence quenching for the F1 against TNT; 32% quenching was observed after 10 seconds and it reached to 87.4% after five minutes. The intense blue emission of the pyrene excimers also enabled the naked-eye detection of the nitroaromatic explosives. Figure 4.14 shows emission of F1 films under UV-light illumination after they were exposed to TNT for different durations. The rapid fluorescence quenching of the films against TNT vapor can be observed from the photographs. Even after exposure to TNT for 30 seconds, there is a considerable decrease in the bright blue emission of F1 and after 5 minutes, almost all emission is quenched.

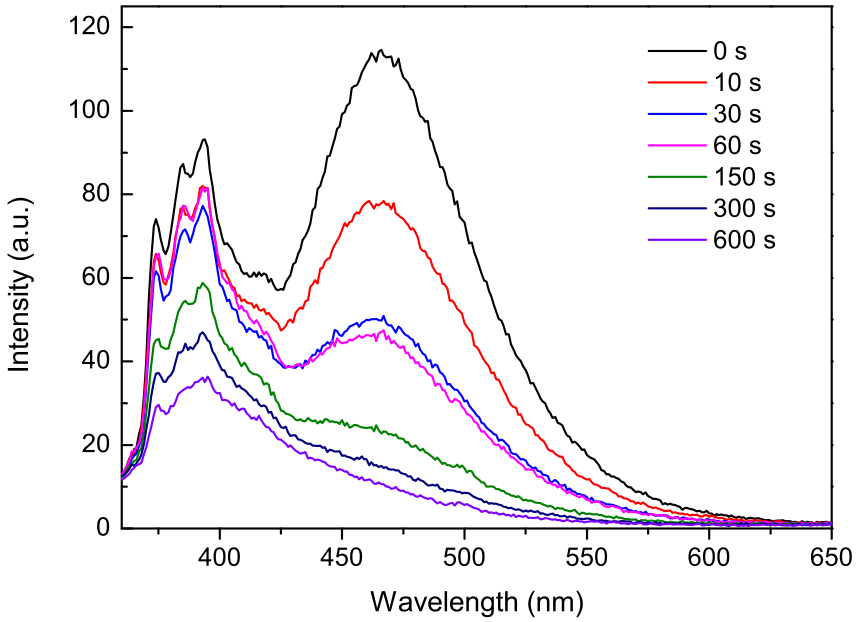

Figure 4.13: Time-dependent fluorescence quenching of the F1 film via exposure to TNT for increasing time.

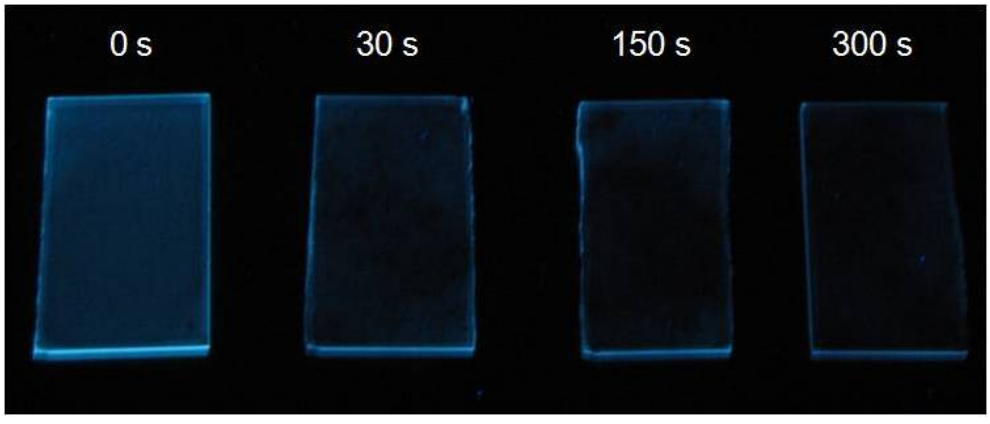

Figure 4.14: Visual detection of TNT vapor. Photographs of F1 films under UV light illumination which were exposed to TNT vapor for different durations as depicted above the films.

Fluorescence of F2 film which is shown in Figure 4.15 was considerably quenched by TNT indicating the film is also suitable for sensing TNT with its bright excimer emission and high quenching signal. Fluorescence of F3 film which is shown in Figure 4.16 was also quenched by TNT, however at a slower rate compared to F1 and F2 films. It is clearly observed that F3 film has very strong excimer emission although it is exposed to TNT for ten minutes indicating that quenching may not be visualized for this film.

Quenching efficiencies of the F1, F2 and F3 films are shown in Figure 4.17 and can be more clearly compared. For the F2 film; 18.2% quenching and 68.2% quenching were observed after 10 seconds and five minutes, respectively. On the other hand for the thicker film, F3; the quenching efficiencies were much lower; as 8.0% and 42.1% after 10 seconds and five minutes, respectively. Fluorescence quenching efficiency is depended on the film thickness and as previously shown, F1; the thinnest film showed the highest quenching efficiency. Higher quenching efficiency for the F1 and F2 films compared to thicker F3 film can be attributed to the higher porosity of these films (Table 4.1) and easier diffusion of TNT molecules through these films.

Fluorescence quenching based TNT sensing with pyrene excimers is illustrated in Figure 4.18. Pyrene doped ormosil film emits light at around 470 nm when it is excited at 340 nm in the absence of TNT. In the presence of TNT, emission of the film is quenched due to the photo-induced electron transfer between TNT and excited pyrene. When TNT interacts with excited pyrene the excited electron is transferred to the LUMO of the TNT molecule instead of relaxing back to the ground state of pyrene. (Figure 4.18) [60].

Sensing measurement with an F2 film was also performed for another nitroaromatic explosive DNT by using the same procedure as we did with TNT. Fluorescence of F2 film which is shown in Figure 4.19 was quenched rapidly against DNT. Quenching efficiencies observed with DNT for 10 s and five minutes are 19.9% and 88.2%, respectively. It is shown in Figure 4.20 that F2 film exhibits higher quenching efficiency against DNT than TNT due to the higher vapor pressure of DNT compared to TNT.

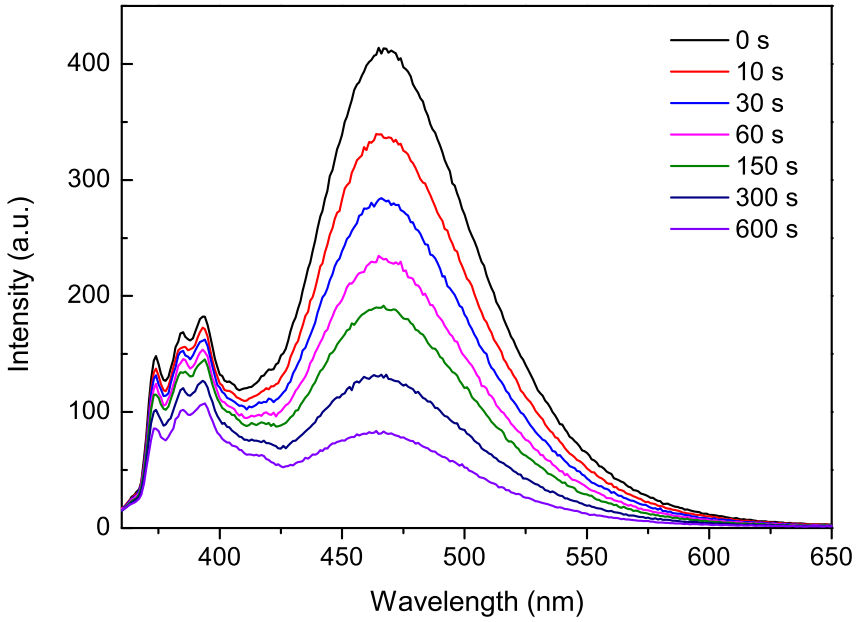

Figure 4.15: Time-dependent fluorescence quenching of the F2 film via exposure to TNT for increasing time.

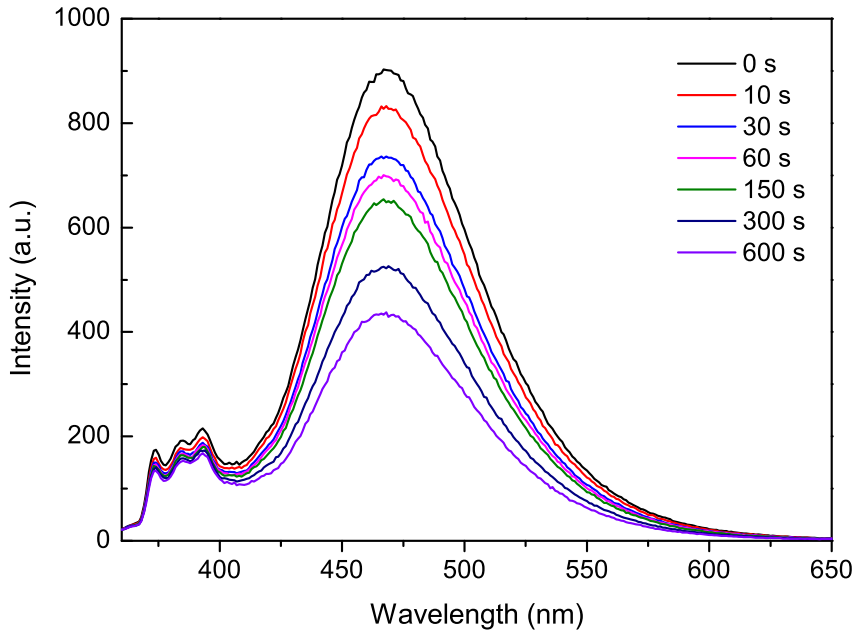

Figure 4.16: Time-dependent fluorescence quenching of the F3 film via exposure to TNT for increasing time.

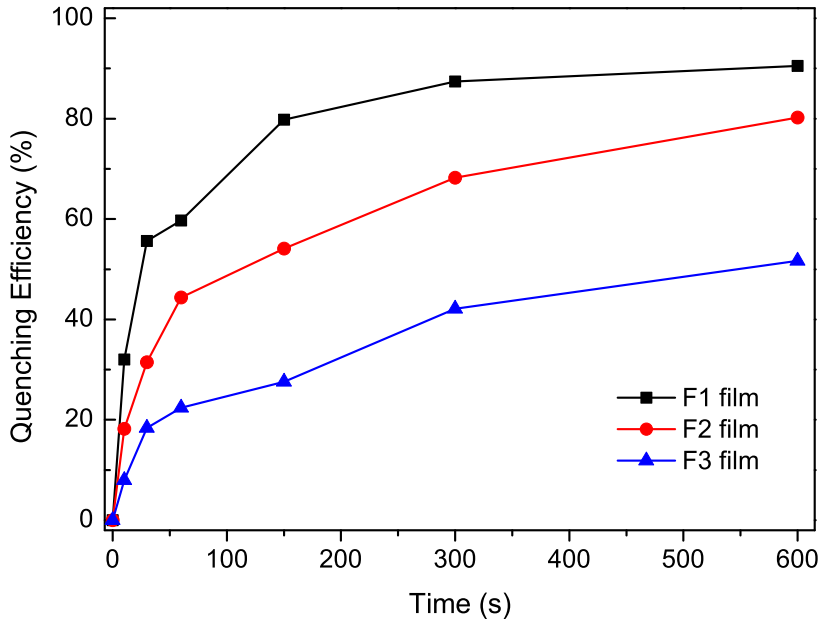

Figure 4.17: Fluorescence quenching efficiencies of the F1, F2 and F3 films (108 nm, 251 nm and 1202 nm, respectively) for different exposure times.

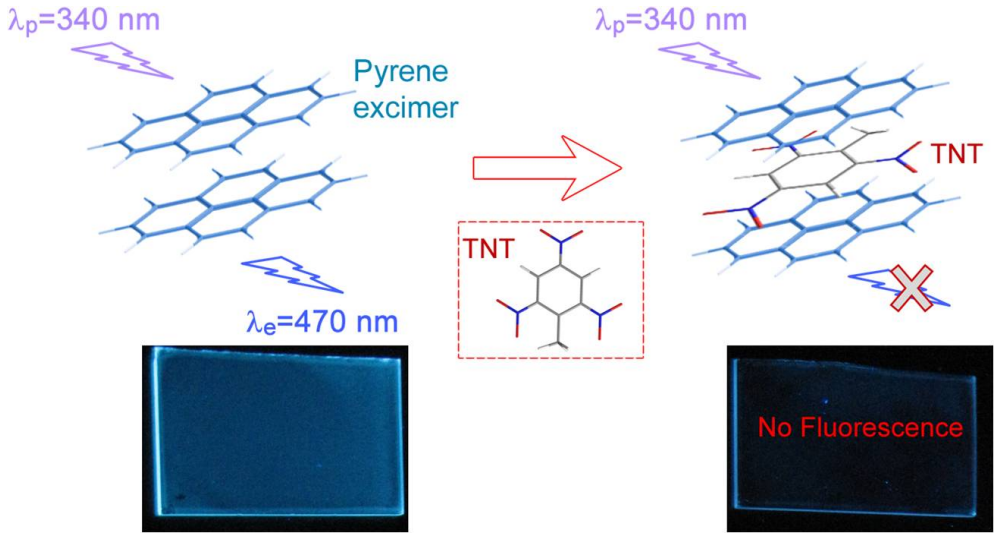

Figure 4.18: Schematic of TNT sensing with pyrene excimer via fluorescence quenching (photographs show the corresponding films under UV light).

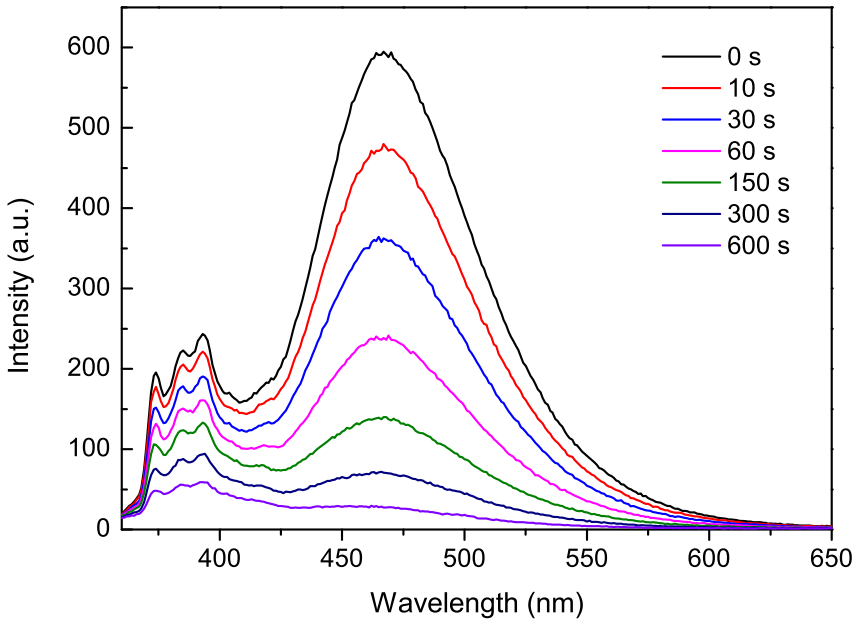

Figure 4.19: Time-dependent fluorescence quenching of the F2 film via exposure to DNT for increasing time.

In order to compare self-quenching of pyrene excimer emission with its quenching in the presence of TNT, we calculated 50% quenching times of initial emissions for F2 film. 50% of the initial excimer emission self-quenches within approximately 6 days (Figure 4.10). On the other hand, in the presence of TNT, 50% quenching takes only $\sim$ 150 seconds (Figure 4.15) indicating that quenching in the presence of TNT is approximately 3 x 10^3 times faster than self-quenching of the excimer emission. Therefore, pyrene doped mesoporous ormosil mesoporous thin films can be used for the sensing of TNT vapor by monitoring the rapid decrease in the excimer emission intensity.

4.4 Selectivity of the Sensor

After demonstrating the sensitivity of the sensor against TNT and DNT vapors, we tested the sensor with nitrobenzene (NB) which is also a nitroaromatic explosive and also with several volatile aromatic or nonaromatic compounds using

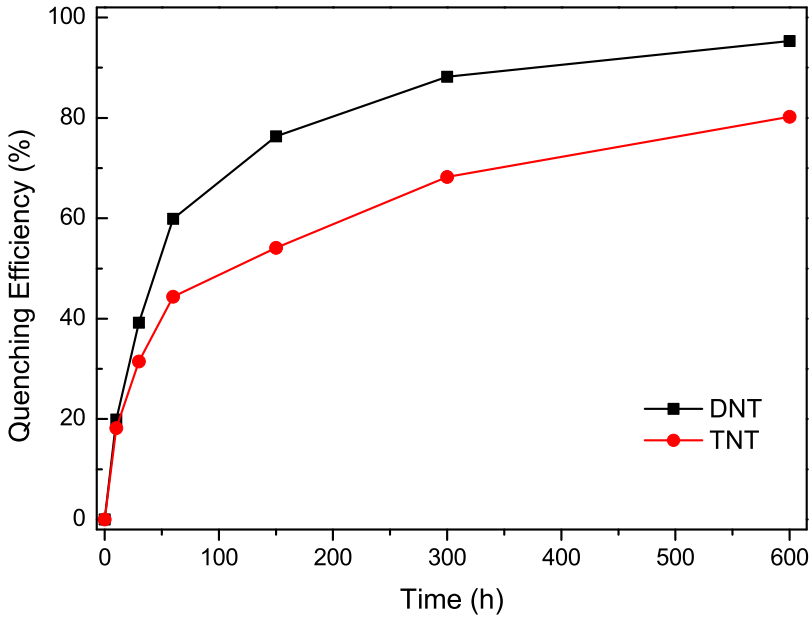

Figure 4.20: Fluorescence quenching efficiency of F2 film via exposure to DNT and TNT with respect to time.

4.14 mM pyrene doped F2 films. Calculated fluorescence quenching efficiencies are shown in Figure 4.21 for all tested compounds including TNT and DNT. Nitroaromatic explosives largely quenched the fluorescence of the F2 film. Fluorescence quenching efficiencies of the films against DNT, TNT and NB were 39.2%, 31.5% and 16.2% after 30 seconds, respectively. After five minutes, fluorescence quenching efficiencies of the films against DNT, TNT and NB were increased to 88.2%, 68.2% and 66.7%, respectively. As mentioned above, higher quenching efficiency of DNT can be attributed to its higher vapor pressure (∼100 ppb) than TNT (∼5 ppb) [69]. On the other hand, NB shows lower quenching efficiency although its vapor pressure (∼150 ppm) is considerably higher compared to TNT and DNT [13]. Beside vapor pressure, the exergonicity of electron transfer between excited pyrene excimers and nitroaromatic compounds and also their binding strength to the pyrene molecules affect quenching performance of nitroaromatics [19, 70]. Binding strength of NB to the electron-rich pyrene rings is expected to be lower than those of TNT and DNT since NB has only one

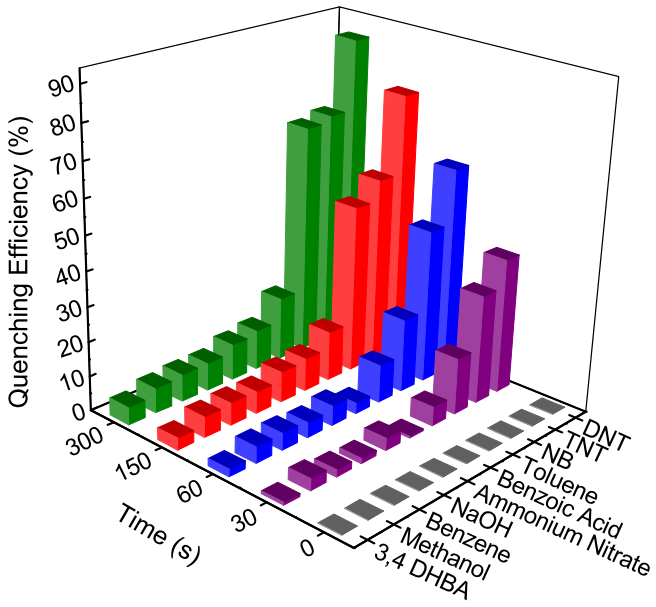

Figure 4.21: Selectivity of the pyrene doped ormosil films for nitroaromatic explosive vapors.

electron-withdrawing nitro group. Therefore NB results in a lower quenching efficiency. Lastly, exposure of the sensor to toluene, ammonium nitrate, benzene, benzoic acid, sodium hydroxide, 3,4 DHBA and methanol did not result in a significant fluorescence quenching indicating the good selectivity of the sensor to nitroaromatic explosives.

4.5 Reusability of the Sensor

Reusability is an important sensor parameter, which is desired to develop cost-effective sensors. With regard to this, we evaluated the reusability of our films. We examined recovery of excimer emission signal of an F2 film after it was quenched with TNT vapor. In order to recover the fluorescence, the quenched film was simply immersed in water for ten minutes and then left to dry at room temperature for another ten minutes. Fluorescence intensities measured after individual quenching and recovery cycles are shown in Figure 4.22(a). In the first

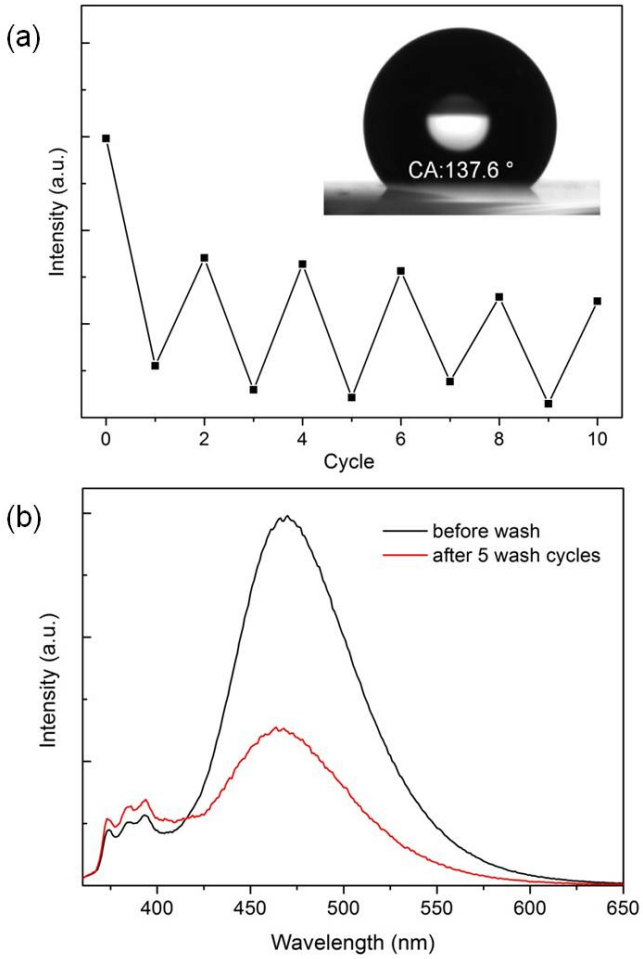

Figure 4.22: Fluorescence quenching and recovery cycles for an F2 film. The inset is the photograph of water droplet on the F2 film with contact angle (CA) value indicating that the film is hydrophobic. (b) Fluorescence spectra recorded before the first quenching and after the fifth recovery step of the tested film.

recovery step, fluorescence of the F2 was not fully recovered. Since the film is hydrophobic as shown in the inset of Figure 4.22(a), presumably water did not penetrate through the pores of the film and consequently did not completely wash the film in the first recovery cycle. Nevertheless, there is a very significant difference in the intensities between the quenched and recovered states which enables accurate sensing of TNT. Interestingly, fluorescence of the F2 film can almost be recovered at least for four additional cycles. As shown in Figure 4.22(b), the film still has a considerably strong excimer emission intensity after the fifth recovery cycle indicating that the film is suitable for further use.

Chapter 5

Conclusion

In this work, we described the preparation of ormosil thin films with bright and stable pyrene excimer emission via a facile sol-gel process. Pyrene molecules were encapsulated in the ormosil network without covalently binding and pyrene excimers were formed in the network. Time-dependent stability of pyrene excimers were investigated in both porous and nonporous ormosil films. Pyrene excimer formation and corresponding emission intensity were monitored using the fluorescence spectroscopy. A significant pyrene excimer emission is observed with pyrene concentration above 2.07 mM and excimer emission is enhanced more with further increasing the pyrene concentration. Interestingly, excimer emission is stronger and more stable in porous films, whereas it is weak and disappears rapidly in nonporous counterparts. Mesoporous structure of ormosil films is believed to be responsible for the improved excimer formation and stability by acting as an ideal environment for nanoscale confinement of pyrene molecules.

In the second part of the thesis, we studied nitroaromatic explosive sensing performance of the porous films. Mesoporous films exhibited rapid fluorescence quenching response against nitroaromatic explosive vapors. Fluorescence quenching efficiency increased with decreasing film thickness due to the higher diffusion rate of analyte vapors through the thinner films. More importantly, fluorescence response of the films can be observed visually under UV light illumination. Films did not demonstrate significant fluorescent quenching response in the presence of

other various analytes, indicating the good selectivity of the sensor to nitroaromatic explosives. Furthermore, fluorescence signal of the films can be regenerated by simply washing the films with water. We demonstrated that the films can be used for at least five quenching-recovery cycles. We believe that pyrene doped mesoporous ormosil thin films present a promising sensor platform with their high surface area, easy synthesis, cost-effectiveness and reusability.

Bibliography

[1] T. M. Figueira-Duarte and K. Mllen, "Pyrene-based materials for organic electronics," *Chem. Rev.*, vol. 111, no. 11, pp. 7260–7314, 2011.

[2] L. Ding and Y. Fang, "Chemically assembled monolayers of fluorophores as chemical sensing materials," *Chem. Soc. Rev.*, vol. 39, pp. 4258–4273, 2010.

[3] F. M. Winnik, "Photophysics of preassociated pyrenes in aqueous polymer solutions and in other organized media," *Chem. Rev.*, vol. 93, no. 2, pp. 587–614, 1993.

[4] Y. Fujiwara and Y. Amao, "Optical oxygen sensor based on controlling the excimer formation of pyrene-1-butylic acid chemisorption layer onto nanoporous anodic oxidized aluminium plate by myristic acid," *Sens. Act. B: Chem.*, vol. 89, no. 12, pp. 58 – 61, 2003.

[5] N. Leventis, I. A. Elder, D. R. Rolison, M. L. Anderson, and C. I. Merzbacher, "Durable modification of silica aerogel monoliths with fluorescent 2,7-diazapyrenium moieties. Sensing oxygen near the speed of open-air diffusion," *Chem. Mater.*, vol. 11, no. 10, pp. 2837–2845, 1999.

[6] A. Ueno, I. Suzuki, and T. Osa, "Host-guest sensory systems for detecting organic compounds by pyrene excimer fluorescence," *Anal. Chem.*, vol. 62, no. 22, pp. 2461–2466, 1990.

[7] J. Huang, Y. Wu, Y. Chen, Z. Zhu, X. Yang, C. J. Yang, K. Wang, and W. Tan, "Pyrene-excimer probes based on the hybridization chain reaction for the detection of nucleic acids in complex biological fluids," *Angew. Chem. Int. Ed.*, vol. 50, no. 2, pp. 401–404, 2011.

[8] R.-H. Yang, W.-H. Chan, A. W. M. Lee, P.-F. Xia, H.-K. Zhang, and L, "A ratiometric fluorescent sensor for Ag^{I} with high selectivity and sensitivity," *J. Am. Chem. Soc.*, vol. 125, no. 10, pp. 2884–2885, 2003.

[9] Y. Suzuki, T. Morozumi, H. Nakamura, M. Shimomura, T. Hayashita, and R. A. Bartsh, "New fluorimetric alkali and alkaline earth metal cation sensors based on noncyclic crown ethers by means of intramolecular excimer formation of pyrene," *J. Phys. Chem. B*, vol. 102, no. 40, pp. 7910–7917, 1998.

[10] J. V. Goodpaster, J. F. Harrison, and V. L. McGuffin, "Ab initio study of selective fluorescence quenching of polycyclic aromatic hydrocarbons," *J. Phys. Chem. A*, vol. 106, no. 44, pp. 10645–10654, 2002.

[11] Y. Wang, A. La, Y. Ding, Y. Liu, and Y. Lei, "Novel signal-amplifying fluorescent nanofibers for naked-eye-based ultrasensitive detection of buried explosives and explosive vapors," *Adv. Func. Mater.*, vol. 22, no. 17, pp. 3547–3555, 2012.

[12] G. B. Demirel, B. Daglar, and M. Bayindir, "Extremely fast and highly selective detection of nitroaromatic explosive vapours using fluorescent polymer thin films," *Chem. Commun.*, vol. 49, pp. 6140–6142, 2013.

[13] H. Bai, C. Li, and G. Shi, "Pyrenyl excimers induced by the crystallization of poss moieties: Spectroscopic studies and sensing applications," *ChemPhysChem*, vol. 9, no. 13, pp. 1908–1913, 2008.

[14] L. Basabe-Desmonts, D. N. Reinhoudt, and M. Crego-Calama, "Design of fluorescent materials for chemical sensing," *Chem. Soc. Rev.*, vol. 36, pp. 993–1017, 2007.

[15] M.-C. Li, R.-M. Ho, and Y.-D. Lee, "Photo-induced excimer formation of pyrene-labeled polymers for optical recording," *J. Mater. Chem.*, vol. 21, pp. 2451–2454, 2011.

[16] S. Pujari, M. Kambale, P. Bhosale, P. Rao, and S. Patil, "Optical properties of pyrene doped polymer thin films," *Mater. Res. Bull.*, vol. 37, no. 9, pp. 1641 – 1649, 2002.

[17] H.-S. Jang, Y. Wang, Y. Lei, and M.-P. Nieh, "Controllable formation of pyrene ($C_{16}H_{10}$) excimers in polystyrene/tetrabutylammonium hexafluorophosphate films through solvent vapor and temperature annealing," *J. Phys. Chem. C*, vol. 117, no. 3, pp. 1428–1435, 2013.

[18] S. Tao, G. Li, and H. Zhu, "Metalloporphyrins as sensing elements for the rapid detection of trace tnt vapor," *J. Mater. Chem.*, vol. 16, pp. 4521–4528, 2006.

[19] S. Tao, J. Yin, and G. Li, "High-performance tnt chemosensory materials based on nanocomposites with bimodal porous structures," *J. Mater. Chem.*, vol. 18, pp. 4872–4878, 2008.

[20] Y. Long, H. Chen, Y. Yang, H. Wang, Y. Yang, N. Li, K. Li, J. Pei, and F. Liu, "Electrospun nanofibrous film doped with a conjugated polymer for dnt fluorescence sensor," *Macromolecules*, vol. 42, no. 17, pp. 6501–6509, 2009.

[21] V. R. Kaufman and D. Avnir, "Structural changes along the sol-gel-xerogel transition in silica as probed by pyrene excited-state emission," *Langmuir*, vol. 2, no. 6, pp. 717–722, 1986.

[22] T. Keeling-Tucker and J. D. Brennan, "Fluorescent probes as reporters on the local structure and dynamics in sol-gel-derived nanocomposite materials," *Chem. Mater.*, vol. 13, no. 10, pp. 3331–3350, 2001.

[23] B. Dunn and J. I. Zink, "Probes of pore environment and molecule-matrix interactions in sol-gel materials," *Chem. Mater.*, vol. 9, no. 11, pp. 2280–2291, 1997.

[24] Q. Deng, Y. Hu, R. B. Moore, C. L. McCormick, and K. A. Mauritz, "Nafion/ormosil hybrids via in situ sol-gel reactions. 3. Pyrene fluorescence probe investigations of nanoscale environment," *Chem. Mater.*, vol. 9, no. 1, pp. 36–44, 1997.

[25] C. J. Brinker and G. W. Scherer, *Sol-Gel Sci.* Elsevier, 1990.

[26] A. Walcarius and L. Mercier, "Mesoporous organosilica adsorbents: nano-engineered materials for removal of organic and inorganic pollutants," *J. Mater. Chem.*, vol. 20, pp. 4478–4511, 2010.

[27] A. Walcarius, "Mesoporous materials and electrochemistry," *Chem. Soc. Rev.*, vol. 42, pp. 4098–4140, 2013.

[28] L. L. Hench and J. K. West, "The sol-gel process," *Chem. Rev.*, vol. 90, no. 1, pp. 33–72, 1990.

[29] G. J. d. A. A. Soler-Illia, C. Sanchez, B. Lebeau, and J. Patarin, "Chemical strategies to design textured materials: from microporous and mesoporous oxides to nanonetworks and hierarchical structures," *Chem. Rev.*, vol. 102, no. 11, pp. 4093–4138, 2002.

[30] C. T. Kresge, M. E. Leonowicz, W. J. Roth, J. C. Vartuli, and J. S. Beck, "Ordered mesoporous molecular sieves synthesized by a liquid-crystal template mechanism," *Nature*, vol. 359, no. 6397, pp. 710–712, 1992.

[31] J. S. Beck, J. C. Vartuli, W. J. Roth, M. E. Leonowicz, C. T. Kresge, K. D. Schmitt, C. T. W. Chu, D. H. Olson, and E. W. Sheppard, "A new family of mesoporous molecular sieves prepared with liquid crystal templates," *J. Am. Chem. Soc.*, vol. 114, no. 27, pp. 10834–10843, 1992.

[32] A. Stein, B. J. Melde, and R. C. Schroden, "Hybrid inorganic-organic mesoporous silicates-nanoscopic reactors coming of age," *Adv. Mater.*, vol. 12, no. 19, pp. 1403–1419, 2000.

[33] T. Wagner, S. Haffer, C. Weinberger, D. Klaus, and M. Tiemann, "Mesoporous materials as gas sensors," *Chem. Soc. Rev.*, vol. 42, pp. 4036–4053, 2013.

[34] Z. Li, J. C. Barnes, A. Bosoy, J. F. Stoddart, and J. I. Zink, "Mesoporous silica nanoparticles in biomedical applications," *Chem. Soc. Rev.*, vol. 41, pp. 2590–2605, 2012.

[35] M. Pagliaro, R. Ciriminna, and G. Palmisano, "Silica-based hybrid coatings," *J. Mater. Chem.*, vol. 19, pp. 3116–3126, 2009.

[36] A. Yildirim, H. Budunoglu, H. Deniz, M. O. Guler, and M. Bayindir, "Template-free synthesis of organically modified silica mesoporous thin films for tnt sensing," *ACS Appl. Mater. Interfaces*, vol. 2, no. 10, pp. 2892–2897, 2010.

[37] S. D. Bhagat, C.-S. Oh, Y.-H. Kim, Y.-S. Ahn, and J.-G. Yeo, "Methyltrimethoxysilane based monolithic silica aerogels via ambient pressure drying," *Mic. Mes. Mater.*, vol. 100, no. 13, pp. 350 – 355, 2007.

[38] A. Vu, J. Phillips, P. Bhlmann, and A. Stein, "Quenching performance of surfactant-containing and surfactant-free fluorophore-doped mesoporous silica films for nitroaromatic compound detection," *Chem. Mater.*, vol. 25, no. 5, pp. 711–722, 2013.

[39] N. Leventis, C. Sotiriou-Leventis, G. Zhang, and A.-M. M. Rawashdeh, "Nanoengineering strong silica aerogels," *Nano Letters*, vol. 2, no. 9, pp. 957–960, 2002.

[40] K. Kanamori and K. Nakanishi, "Controlled pore formation in organotrialkoxysilane-derived hybrids: from aerogels to hierarchically porous monoliths," *Chem. Soc. Rev.*, vol. 40, pp. 754–770, 2011.

[41] Z. Yang, Y. Lu, and Z. Yang, "Mesoporous materials: tunable structure, morphology and composition," *Chem. Commun.*, vol. 0, pp. 2270–2277, 2009.

[42] Y. Lu, "Surfactant-templated mesoporous materials: From inorganic to hybrid to organic," *Angew. Chem. Int. Ed.*, vol. 45, no. 46, pp. 7664–7667, 2006.

[43] A. C. Pierre and G. M. Pajonk, "Chemistry of aerogels and their applications," *Chem. Rev.*, vol. 102, no. 11, pp. 4243–4266, 2002.

[44] S. S. Kistler, "Coherent expanded aerogels and jellies," *Nature*, vol. 127, no. 1, pp. 741–741, 1931.

[45] S. S. Kistler, "Coherent expanded-aerogels," *J. Phys. Chem.*, vol. 36, no. 1, pp. 52–64, 1931.

[46] S. S. Prakash, C. J. Brinker, A. J. Hurd, and S. M. Rao, "Silica aerogel films prepared at ambient pressure by using surface derivatization to induce reversible drying shrinkage," *Nature*, vol. 374, no. 6521, pp. 439–443, 1995.

[47] H. Budunoglu, A. Yildirim, M. O. Guler, and M. Bayindir, "Highly transparent, flexible, and thermally stable superhydrophobic ormosil aerogel thin films," *ACS Appl. Mater. Interfaces*, vol. 3, no. 2, pp. 539–545, 2011.

[48] A. Yildirim, H. Budunoglu, M. Yaman, M. O. Guler, and M. Bayindir, "Template free preparation of nanoporous organically modified silica thin films on flexible substrates," *J. Mater. Chem.*, vol. 21, pp. 14830–14837, 2011.

[49] F. Ye, M. M. Collinson, and D. A. Higgins, "What can be learned from single molecule spectroscopy? Applications to sol-gel-derived silica materials," *Phys. Chem. Chem. Phys.*, vol. 11, pp. 66–82, 2009.

[50] J. B. Birks, "Excimers," *Rep. Prog. Phys.*, vol. 38, no. 8, p. 903, 1975.

[51] M. E. Ostergaard and P. J. Hrdlicka, "Pyrene-functionalized oligonucleotides and locked nucleic acids (LNAs): Tools for fundamental research, diagnostics, and nanotechnology," *Chem. Soc. Rev.*, vol. 40, pp. 5771–5788, 2011.

[52] T. Umemoto, P. J. Hrdlicka, B. R. Babu, and J. Wengel, "Sensitive SNP dual-probe assays based on pyrene-functionalized 2'-amino-LNA: Lessons to be learned," *ChemBioChem*, vol. 8, no. 18, pp. 2240–2248, 2007.

[53] T. Liu, L. Ding, K. Zhao, W. Wang, and Y. Fang, "Single-layer assembly of pyrene end-capped terthiophene and its sensing performances to nitroaromatic explosives," *J. Mater. Chem.*, vol. 22, pp. 1069–1077, 2012.

[54] H. Du, G. He, T. Liu, L. Ding, and Y. Fang, "Preparation of pyrene-functionalized fluorescent film with a benzene ring in spacer and sensitive detection to picric acid in aqueous phase," *J. Photochem. and Photobiol. A: Chem.*, vol. 217, no. 23, pp. 356 – 362, 2011.

[55] D. Moore, "Recent advances in trace explosives detection instrumentation," *Sens. Imag. Int. J.*, vol. 8, no. 1, pp. 9–38, 2007.

[56] D. S. Moore, "Instrumentation for trace detection of high explosives," *Rev. Sci. Instrum.*, vol. 75, no. 8, pp. 2499–2512, 2004.

[57] S. Singh, "Sensors-an effective approach for the detection of explosives," *J. Hazard. Mater.*, vol. 144, no. 12, pp. 15 – 28, 2007.

[58] Y. Salinas, R. Martinez-Manez, M. D. Marcos, F. Sancenon, A. M. Costero, M. Parra, and S. Gil, "Optical chemosensors and reagents to detect explosives," *Chem. Soc. Rev.*, vol. 41, pp. 1261–1296, 2012.

[59] S. Z. Nergiz, N. Gandra, M. E. Farrell, L. Tian, P. M. Pellegrino, and S. Singamaneni, "Biomimetic sers substrate: peptide recognition elements for highly selective chemical detection in chemically complex media," *J. Mater. Chem. A*, vol. 1, pp. 6543–6549, 2013.

[60] S. J. Toal and W. C. Trogler, "Polymer sensors for nitroaromatic explosives detection," *J. Mater. Chem.*, vol. 16, pp. 2871–2883, 2006.

[61] K.-S. Focsaneanu and J. C. Scaiano, "Potential analytical applications of differential fluorescence quenching: pyrene monomer and excimer emissions as sensors for electron deficient molecules," *Photochem. Photobiol. Sci.*, vol. 4, pp. 817–821, 2005.

[62] S. Tao, G. Li, and J. Yin, "Fluorescent nanofibrous membranes for trace detection of tnt vapor," *J. Mater. Chem.*, vol. 17, pp. 2730–2736, 2007.

[63] S. Tao, Z. Shi, G. Li, and P. Li, "Hierarchically structured nanocomposite films as highly sensitive chemosensory materials for tnt detection," *ChemPhysChem*, vol. 7, no. 9, pp. 1902–1905, 2006.

[64] Y. Yang, H. Wang, K. Su, Y. Long, Z. Peng, N. Li, and F. Liu, "A facile and sensitive fluorescent sensor using electrospun nanofibrous film for nitroaromatic explosive detection," *J. Mater. Chem.*, vol. 21, pp. 11895–11900, 2011.

[65] S. Tao and G. Li, "Porphyrin-doped mesoporous silica films for rapid tnt detection," *Coll. Polymer Sci.*, vol. 285, no. 7, pp. 721–728, 2007.

[66] K. Kokado, T. Iwamura, and Y. Chujo, "Synthesis and photoluminescence properties of pyrene-incorporated organic-inorganic polymer hybrids," *Polym. J*, vol. 40, no. 5, pp. 402–408, 2008.

[67] R. Dabestani, M. Kidder, and A. C. Buchanan, "Pore size effect on the dynamics of excimer formation for chemically attached pyrene on various silica surfaces," *J. Phys. Chem. C*, vol. 112, no. 30, pp. 11468–11475, 2008.

[68] M. Sluch, A. Vitukhnovsky, and M. Petty, "Pyrene excimer formation in langmuir-blodgett films," *Thin Solid Films*, vol. 284285, no. 0, pp. 622 – 626, 1996.

[69] A. Rose, Z. Zhu, C. F. Madigan, T. M. Swager, and V. Bulovic, "Sensitivity gains in chemosensing by lasing action in organic polymers," *Nature*, vol. 434, no. 7035, pp. 876–879, 2005.

[70] J.-S. Yang and T. M. Swager, "Fluorescent porous polymer films as tnt chemosensors: Electronic and structural effects," *J. Am. Chem. Soc.*, vol. 120, no. 46, pp. 11864–11873, 1998.